Quantum Dot Peptide Nanobioassembly for Biosensing

2018

Sreenadh Sasidharan Pillai

Contents

Chapter 1. Introduction

Matrix metalloproteinases (MMPs) are a group of endopeptidases.[1–3] The name MMP originates from the catalytic dependence of the enzymes on zinc ions and their extraordinary capability to disintegrate the structural elements of extra cellular matrix (ECM).[4] MMPs play an important role in angiogenesis, development, wound healing also pathology such as cancer and arthritis.[5] Larger quantity of MMPs are expressed inside and the ECM of cancer cells than normal cells, high rise in expression are observed at the interaction region plane of tumour- stroma.[6] Tumour progression is apparently depend on angiogenesis[7,8] and MMP-2 mediate tumor angiogenesis.[9] MMP-2 is secreted as proMMPs by fibroblasts and are either discharged to the extracellular matrix or docked to integrin receptors. P. C. Brooks *et al*., revealed the localization of MMP-2 on the surface of cancer cells in the active form through interaction with αvβ3 integrin receptors.[10] As proved by J.L. Seltzer *et al*., short peptide containing PLGVR amino acid sequence could target MMP-2.[11] The extracellular matrix receptors integrin are group of adhesion molecules composed of non-covalently correlated α and β chains assembles to form diverse heterodimers with characteristic cellular and adhesive specificities.[12] These receptors were involved in *in vitro* cell adhesion and migration.[13] The reality is αvβ3 maintain cell motility while MMP-2 potentiates extracellular matrix degradation which substantiates that these proteins function in a cooperative manner to stimulate the invasive behavior of cells during tissue remodeling, inflammation, development, and cancer.[8] The extracellular matrix (ECM) prevails as a dynamic niche in cancer development. Cellular invasion depends on adhesion as well as proteolytic modification of the extracellular matrix.

Hence deregulated ECM dynamics are a hallmark of cancer.[14] Here is the crucial point, if one could sense and image the deregulated ECM dynamics from the excessive amount of MMP-2 presence with the aid of the PLGVR amino acid sequence MMP-2 target peptide. Hence simultaneous sensing and imaging of MMP-2 localization at cancer cell surface will further develop new theranostics interventions and novel strategy for tissue engineering and regenerative medicines. Here demands the development of a supersensitive MMP-2 detecting biosensor.

The applicability of conventional fluorescent probe is limited in biosensing because they generally display only modest fluorescence changes upon sensing, thus providing insufficient resolution. The degree of resolution mainly depends on the fluorescence-quenching efficiency and target specificity of the probe. Therefore, a high luminescence quenching efficiency and specific recognition properties of the target biomolecule are essential for the development of supersensitive luminescence based probes for both biosensing as well as imaging complex system like living cells.

Semiconductor nanocrystals, specifically CdSe/ZnS quantum dots are intelligent materials having wide spectrum of application in the modern technological world such as solar cells,[15] semiconductor LASERs,[16,17] single photon sources,[18,19] Light Emitting Diodes,[20] 4K and 8K displays technologies[21] and other scientific interventions such as bioanalysis,[22–24] single molecule bioimaging,[25] STED microscopy[26] etc. Quantum dots are efficient donor material for Förster resonance energy transfer (FRET) processes[27] and is a sophisticated tool for fluorescence-based detection and imaging of biomolecules and biosystems, for example protein-protein

interaction, ligand receptor interaction, protein–DNA interaction etc.[28,29] QDs have some unique optical properties compared to the regular fluorophores like organic dyes, fluorescent polymers, chemiluminescent substrates, fluorescent proteins, etc. and that include wide excitation window and narrow emission which help to block the overlap between donor-acceptor emission-absorption spectra consequently prevent the acceptor emission from direct excitation, which potentiate distinct advantages in bioanalytical and imaging application.[30–37] QDs are bright emitters and can feature narrow symmetric emission spectra with a full width at half maximum ~25-40 nm and it is tunable throughout the visible spectrum, possessing long excited state life time with exceptional photostability aside from blinking with power law statistics or fluorescence intermittency, so they can be switched between their ground (off) and luminescent (on) state again and again.[38–40] Despite several reports on bioimaging and biosensing applications of QDs, controlled and targeted detection of biomolecules using quantum dots is an ongoing challenge. When a QD is conjugated with a spectrally suitable chromophore, which can be a fluorescent or a non-fluorescent dye molecule, QD luminescence can be quenched by Förster resonance energy transfer (FRET) to the quencher dye. If we use a fluorescent dye molecule as acceptor, the FRET from QD to dye will quench the luminescence of QD and will glow the acceptor fluorescence hence there is a chance of acceptor fluorescence as back ground signal at the time of detection, which can reduce the resolution, but if we use a non fluorescent dye molecule we can avoid such acceptor fluorescence in the back ground up on sensing.

In this thesis, an inorganic QD donor material and organic non fluorescent black hole quencher-1(BHQ-1) dye molecule were assembled through a bridging matrix

metalloproteinase-2 (MMP-2) target peptide, forming a nanobioassembly. The synthesis and characterization of QD peptide based nanoassemblies with MMP-2 target peptide were described in Chapter 2. Förster resonance energy transfer (FRET) mediated photoluminescence quenching of QDs were confirmed in a stoichiometrically assembled QD-peptide- Black hole quencher (BHQ-1) nanoassembly through steady state and time-resolved spectroscopy. The results were analyzed on the theoretical and experiential background of FRET mechanism as well as photophysical properties of QDs. The bioconjugation of QD-peptide-BHQ-1 nanobioassembly on a mesoporous silica nanoparticle (MSN) were described in Chapter 3. Transmission electron microscopic images (TEM) of MSN as wells as MSN-QD-peptide-BHQ-1 conjugates morphologies confirms the formation of MSN-$\{QD\text{-}(pep\text{-}BHQ\text{-}1)_n\}_N$ nanobioassembly. Further the steady state and time resolved measurements gives the quantitative information of FRET mediated photoluminescence quenching in the nanobioassembly. Optical sensing of MMP-2 described in Chapter 4. Highly sensitive detection of MMP-2s were achieved both in solution as well as extra cellular matrix (ECM) of cancer cells with the QD-peptide-BHQ-1 nanobioassembly. The MMP-2 presence at the ECM of H1299 cancer cells were imaged with a multiphoton confocal microscope. Finally chapter 5 is dedicated to concluding remarks and future perspectives.

Chapter 2. Quantum Dot Peptide Nanoassembly

2.1 Introduction

QDs have wide application as an optical imaging agent in biology where they exhibit stable photophysical properties unresponsive to the various components in their surroundings.[41] But this study examines the sensitive QDs photophysical process due to the interaction with different species in their environment. In order to study that the QD surface is modified with a peptide conjugate,[42] which interact physically or chemically with the external bio-chem molecular species. A signal transduction channel between QDs and the peptide conjugate is established primarily through energy transfer between the QDs and the conjugate, here the QD functioning as energy transfer donor and the peptide conjugated on its surface act as acceptor.

Energy transfer from an inorganic QD donor to an organic molecule acceptor was explained by Willard and co-workers.[43,44] A stimulating experiment on energy transfer between QDs and dye molecule has been achieved by Mattoussi group.[45,46] Single molecule level observation of FRET between QD donor and dye acceptors has reported by Hong *et al*.[47] Zhou *et al*. directly conjugated a dye labeled DNA acceptor to QD through a thiol linker.[48] FRET from an organic dye to CdSe QD is experimentally impossible because the radiative decay rate of the dye donor excitation is fast compared to the decay rate for FRET from dye to QD acceptor and also QD could be directly excited, hence it could be difficult to substantiate the FRET to the observed QD emission. But in order to check the lifetime of donor limit the FRET, a dye with a long excited state has used by Clapp *et al*. and confirmed the quenching of dye excitation

lifetime, confirming the FRET from dye donor to QD acceptor.[49] This chapter discusses the synthesis of QD-pep-BHQ-1 nanobioassembly and evaluated energy transfer processes between donor and acceptor.

a) Photoluminescence of CdSe and CdSe/ZnS quantum dots

Quantum dots (QDs) are semiconductor crystalline particles encompasses around 100-10,000 atoms with a dimension comparable with or smaller than the exciton size in the bulk semiconductor.[50–53] The quantum size effect due to the smaller size of nanocrystals affects the spatial confinement of electronic wave function which directly influences the electronic energies.[54–56] Once the quantum dot gets photoexcited it finally relaxes to ground state, but before that it goes through intra band relaxation and decay back to the lowest exciton state in less than 1 ps followed by inter-band relaxation.[57] The inter-band relaxation includes radiative carrier recombination at the band-edge, phonon assisted non-radiative relaxations, non-radiative Auger recombination, or radiative and non-radiative recombination at the surface defects.[58–63] Here the radiative recombination at the band edge is the reason for size dependent tunable photoluminescence. The band edge or lowest exciton state ($1S_{3/2}$ $1S_e$) of CdSe QDs with wurtzite crystal structure split into two fourfold degenerate level due to the internal crystal field generated from anisotropy in the internal crystal structure and the shape asymmetry components of the dots compared to the spherical band approximation in spherical dots.[64–67] The band edge state is further split by electron hole exchange interaction. Hence the initial eightfold degenerate band edge exciton is split into five states represented as total exciton angular momentum projection (quantum number) after the inclusion of anisotropy and exchange interaction within the frame work of perturbation theory for CdSe QDs, $J_m = m_e + m_h$ where $m_{e(h)}$ is the electron (hole) spin

projection. $J_m = \pm 2, \pm 1, 0$ for $1S_{3/2}$ and $J_m = \pm 1, 0$ for 1Se states. Here the $J_m = \pm 2$ and $J_m = 0$ (lower state) are spin forbidden state or optically passive within the electric dipole approximation.[68] Hence the photoactivation of CdSe QDs close to the band edge selectively populate $J_m = \pm 1$ state. The decay of exciton from these states is occur through non-radiative relaxation to the dark exciton state followed by either radiative or non-radiative exciton recombination to the ground state also there is a chance it can thermalize back to the next highest spin allowed state. The involvement of spin forbidden optically passive dark exciton state as well as surface trap state lengthened the average photoluminescence lifetime of CdSe QDs.[69] Non-radiative relaxation at the surface states contributes to poor photoluminescence quantum efficiencies of CdSe QDs. The suppression of surface state with ZnS shells[70] as well as different physical and chemical methods to improve the quantum efficiency of CdSe quantum dots are described in details in the following references for further reading.[71–78]

b) Förster Resonance Energy Transfer

Resonance energy transfer (RET) elucidates a non-radiative energy transfer from an excited donor molecule (D^{ex}) to an acceptor molecule (A). A primary classical mechanism was put forwarded by Jean-Baptiste Perrin,[79,80] and after that his son Francis Perrin proposed a quantum mechanical monograph.[81] But it generates ambiguous results fundamentally because it hypothesized that the donor and acceptor molecule have a discrete fluorescence frequency also he couldn't quantitatively evaluate the accurate value of molecular collision time. In 1946 Theodor Förster come up with classical formalism combining the experimentally easy obtained values such as absorption spectra, fluorescence spectra and excited state life times.[82] But in 1948 Förster came with quantum mechanical description, which is one of the most cited work

about resonance energy transfer so far.[83] This is one of the possible reason why RET is particularly associated with Theodor Förster. But his 1959 paper deals with more conceptual understanding of the FRET process rather than the rigorous theoretical treatment in 1948 paper.[84] In the first two papers he discusses the FRET between like molecules, that is the theory of homotransfer, but in 1949 paper,[85] he accentuates heterotransfer, that is FRET between unlike molecules. The 1965 paper is the extension of quantum mechanical theory introduced in his 1948 paper distinctively explains why the very weak coupling is the basis of FRET processes.[86]

Theodor Förster's theory of resonance energy transfer has established diverse applications in photophysics, photochemistry, photobiology, and many other fields of science, because it allow one to determine the distance between two suitable chromophore, an energy donor and an acceptor, separated in the 1-10 nm range. Förster resonance energy transfer is used as a spectroscopic ruler in bioanalytical application.[87,88] The currently existing abbreviation such as Förster or fluorescence Resonance Energy Transfer (FRET), luminescence (LRET) and bioluminescence (BRET) all are work under a common mechanism of induction of a dipole oscillation in acceptor molecule by the excited donor molecule via Coulombic interactions. As FRET is the approved abbreviation it will be used throughout this work.

i) Theoretical background

Most of the theory mentioned in this chapter has been taken from references.[89,90] For the energy difference ΔE between HOMO and LUMO of acceptor and donor as shown in Figure 1, the following resonance condition has to be accomplished.

$$\Delta E(D \rightarrow D^{ex}) = \Delta E(A \rightarrow A^{ex}) \quad (1)$$

For the establishment of FRET need to satisfy few conditions

1. Strong electronic transitions ability of donor and acceptor.

2. Sufficient spectral overlap must exist between donor emission and acceptor absorbance.

3. Donor and acceptor should keep a proximal distance, but should not touch due to the dipole-dipole feature of interaction.

4. There should be a distinct mutual orientation between dipoles and it should not orient mutually perpendicular

5. High quantum yield of the donor material.

The fundamental entities of Förster's theory are as follows

k_T = rate of energy transfer

τ_D = lifetime of the donor excited state in the absence of acceptor

r_{DA}= the distance between donor and acceptor

R_0 = Förster distance, that is, the donor acceptor distance at which $k_T = 1/\tau_D$, so that at that particular distance, the probability of the excited donor to fluoresce is equal to the probability of transfer of energy to the acceptor.

E = efficiency of transfer

J = overlap integral

κ^2 = orientation factor

Φ_D = quantum yield of the donor fluorescence in the absence of acceptor.

n = refractive index of medium.

Constants in Förster's theory are as follows:

π = 3.141592654

ln 10 = 2.302585093

N_A = 6.0221415 × 10^{23} per mole (actually, Förster used N' = 6.0221415 × 10^{20} per millimole)

The conclusion of Förster theory can be conveniently written as the following set of three equations:

The FRET efficiency E is proportional to sixth power of r and is described

$$E = \frac{k_T}{k_T + {}^1/_{\tau_D}} = \frac{R_0^6}{R_0^6 + r_{DA}^6} \qquad (2)$$

The energy transfer rate is given by

$$k_T = \left(\frac{1}{\tau_D}\right)\left(\frac{R_0}{r_{DA}}\right)^6 \qquad (3)$$

$$R_0 = \left(\frac{9ln(10)\kappa^2\Phi_D}{128\pi^5 n_r^4 N_A} J(\lambda)\right)^{1/6} = 0.02108(\kappa^2\Phi_D n_r^{-4} J(\lambda))^{1/6} \quad \text{nanometer} \qquad (4)$$

where τ_D is the luminescence decay time of donor D in the absence of the acceptor and R_0 is the so called Förster radius, the distance between the donor and acceptor point dipole at which FRET is 50% efficient.

Determination R_0 requires quantities such as the spectral overlap integral of donor emission and acceptor absorption ($J(\lambda)$), the dipole orientation factor between the donor and acceptor (κ^2), the donor quantum yield (Φ_D) and the index of refraction of the surrounding medium (n_r) have to be known.

In this equation R_0 is in Å and $J(\lambda)$ is in $M^{-1}cm^{-1}nm^4$. The dipole orientation factor describes the orientation of transition dipole moments of D^{ex} and A (Figure 2).

In general, κ^2 can range from 0 to 4 and is equal to 2/3 for randomly oriented system in solution. The rates of energy transfer from the α-th excited donor molecule to μ-th molecule of the acceptor; depends on the mutual orientation factor of the dipole moment of the molecule D_α and A_μ

$$\chi_{\alpha\mu} = (d_\alpha . a_\mu) - \frac{3}{r_{\alpha\mu}^2}(d_\alpha . r_{\alpha\mu})(a_\mu . r_{\alpha\mu}) \qquad (5)$$

$$\chi_{\alpha\mu}{}^2 = \left|(d_\alpha . a_\mu) - \frac{3}{r_{\alpha\mu}^2}(d_\alpha . r_{\alpha\mu})(a_\mu . r_{\alpha\mu})\right|^2$$

$$\chi_{\alpha\mu}{}^2 = \left|(\hat{d}_\alpha . \hat{a}_\mu) - 3(\hat{d}_\alpha . \hat{r}_{\alpha\mu})(\hat{a}_\mu . \hat{r}_{\alpha\mu})\right|^2$$

$$\chi_{\alpha\mu}{}^2 = [3\cos\theta_a \cos\theta_d - \cos\varphi]^2$$

$$= [2\cos\theta_a \cos\theta_d - \cos\varphi \sin\theta_a \sin\theta_d]^2$$

Here, θ_a and θ_d are the angles between the donor and acceptor dipoles and the connecting vector **r**, φ is the angle between the two dipoles, or the angle between the planes formed by the donor dipoles and **r** and the acceptor dipole and **r**, see figure 2.

If the donor and acceptor can freely rotate, one obtains an averaged value for $\langle \chi_{\alpha\mu}{}^2 \rangle$ as

$$\langle \chi_{\alpha\mu}{}^2 \rangle = [2\cos\theta_a \cos\theta_d - \cos\varphi \sin\theta_a \sin\theta_d]^2$$

$$= \langle 4\cos^2\theta_a \cos^2\theta_d - 4\cos\theta_a \cos\theta_d \cos\varphi \sin\theta_a \sin\theta_d + \cos^2\varphi \sin^2\theta_a \sin^2\theta_d \rangle$$

$$= \frac{4}{9} + \frac{1}{2}\frac{4}{9} = \frac{2}{3}$$

i.e $\kappa^2 = 2/3$

Two parallel dipole orientation yields the highest FRET efficiency, but at the same time two mutually perpendicular dipole orientation curtail the energy transfer to zero, even with a substantial spectral overlap. The fundamental aspects of dipole-dipole orientation has described in reference.[91]

The spectral overlap integral is estimated using equation 6 where $F_D(\lambda)$ normalized luminescence spectrum of donor, its unit is nm^{-1}, that is should obey the condition of $\int F_D(\lambda)d\lambda = 1$, the $\varepsilon_A(\lambda)$ term represent the extinction coefficient values of the acceptor with unit $M^{-1}cm^{-1}$at various wavelength and λ indicate the wavelength spectrum in nm.

$$J(\lambda) = \int_0^{\alpha} F_D(\lambda)\varepsilon_A(\lambda)\lambda^4 d\lambda \qquad (6)$$

Experimental evaluation of FRET efficiency E is resolved from both steady state and time resolved luminescence measurement.

$$E = 1 - \frac{F_{DA}}{F_D} \text{ (steady state)} \qquad (7)$$

$$E = 1 - \frac{\tau_{DA}}{\tau_D} \text{ (time resolved)} \qquad (8)$$

where F_{DA} and F_D are the donor luminescence intensity in the absence and presence

of acceptor. Similar way τ_D and τ_{DA} are the donor excited state lifetime in the absence and presence of acceptor. Experimentally FRET is revealed from the decrease of donor average life time and intensity if the acceptor is a non emitter but with a concomitant enhancement of acceptor.[82]

c) Luminescence quenching

Luminescence quenching means a process which reduces the luminescence intensity of a sample. Besides FRET, there are other processes such as collisional quenching, excited state reactions, ground state complex formation and molecular rearrangements could change the luminescence intensity and excited state life time of luminophores. There are different luminescence quenching processes, which can be static quenching (example: Formation of nonluminescent complexes by binding interaction luminophores and quencher molecule). Another one is dynamic quenching (example: here there will be no binding interaction but luminophores and quencher will collide each other and quenching happens with respect to diffusive process). These two processes could be described by the Stern-Volmer equation[82]

$$\frac{L_0}{L} = 1 + K_{SV}[Q] \qquad (9)$$

In this equation L_0 and L represent the intensities in the absence and presence of quencher, K_{SV} means the Stern -Volmer constant and [Q] indicate the concentration of the quencher concentration.

If the quenching is dynamic Stern-Volmer quenching constant is represented as K_D

$$\frac{L_0}{L} = \frac{\tau_0}{\tau} = 1 + k_q\tau_0[Q] = 1 + K_D[Q] \qquad (10)$$

where τ_o is the luminescence decay lifetimes in the absence of the quencher and τ represent the value in presence of the quencher and k_q is the bimolecular quenching constant.

For combined static and dynamic quenching the Stern-Volmer equation can be modified to the form

$$\frac{L_0}{L} = (1 + K_D[Q])(1 + K_S[Q]) \qquad (11)$$

If the dynamic and static quenching happens for the same luminophore the second order Stern-Volmer equation shows an upward curvature. More detailed theoretical and practical applications are described in reference[82].

2.2 Materials

a) Donor

Streptavidin conjugated CdSe/ZnS QD having photoemission maximum at 525 nm (QD525), 565 nm (QD565) and 585 nm (QD585) and 655 nm (QD655) Life Technologies (Tokyo, Japan). A 3 nM sample of streptavidin-QD585 has made with milli-Q water (Millipore Milli-Q Lab purification system, Tokyo, Japan). These QDs having large surface to volume ratio, streptavidin peptide were randomly conjugated at the QD surfaces through carbodiimide (EDC) coupling chemistry. Each of these QD accommodates 5 to 10 streptavidin at its surfaces. These streptavidin contain 4 biotin binding site. Hence presumably each QD could accommodate a maximum of 40

number of biotin-(pep-BHQ-1) conjugate.

b) Acceptor

A peptide of the form biotin-GPLG↓VRG(Lys[BHQ-1])-$CONH_2$, with 99% purity was designed and custom made from Custom Peptide & Antibody Service, Eurofins Genomics K.K. (Tokyo, Japan). The peptide contains PLGVR amino acid sequences which function as a MMP-2 target. A 1 mM sample of biotin-pep-BHQ-1 has made in DMSO and diluted further in other medium with respect to the experiments.

2.3 Methods

a) Bioconjugation

Figure 3 describes the schematic illustration of bioconjugation processes. A titration experiment was conducted with distinct ratio of the biotin-pep-BHQ-1 acceptors to a 3 nM concentration solution of QD585. A 2 µM sample of biotin-pep-BHQ-1 pipetted into the cuvette containing 200 µL of 3 nM concentrated QD585. The experiment resulted the formation QD-pep-BHQ-1 nanobioassembly. Every single step of titration manifest a single QD-$(pep\text{-}BHQ\text{-}1)_n$ nanobioassembly construct, where n is the number of moles of biotin-peptide-BHQ-1per QD concentration in solution.

b) Steady state photoluminescence spectroscopy

Photoluminescence of QDs and QDs585-pep-BHQ-1 nanobioassembly were carried out with a fluorescence spectrophotometer F-4500 Hitachi (Tokyo, Japan). But a Fluorolog 3 Horiba, (Tokyo, Japan) spectrophotometer was used to measure the PL of QDs655, QDs525, QDs565 and their corresponding QD-$(pep\text{-}BHQ\text{-}1)_n$ nanobioassembly. The PL spectra were recorded by a CCD detector. The photographs of PL quenching of QDs at various acceptor concentration were taken using an ordinary digital camera.

c) Time resolved photoluminescence spectroscopy

A 800 nm wavelength laser pulses having 200 kHz frequency from a regenerative amplifier (Reg A 9000, Coherent, Japan) seeded by a mode locked Ti: sapphire laser (Mira 900F, Coherent) pumped to optical parametric amplifier (OPA) (OPA 9400, Coherent Japan) and the second- harmonic generation (SHG) crystal in it generate a 400 nm wavelength laser pulses (150 fs) to excite the QD samples. QDs585 photoemission collected with an appropriate band-pass filter and directed to the entrance slit of the polychromator. An assembly of the polychromator (250IS, Chromex, Japan) and a photon counting streak-camera (C4334, Hamamatsu, Japan) were used to record time resolved PL decay lifetime of QDs585.

2.4 Results and Discussion

a) Steady state photoluminescence measurement

The cuvette for photoluminescence spectroscopic measurements were first rinsed using acetone and ethanol, then socked in aqueous H_2SO_4 for one hour, after that washed with milli-Q water several times and finally dried in a nitrogen flow. A 200 μL sample of QD585 at 3 nM concentration has taken in an optical cuvette. It first excited at 400 nm and the PL profiles were recorded. Further a 2 μL of biotin-pep-BHQ-1 with 30 nM concentrations were titrated against the QD samples within one minute time interval for the successive excitation and the procedure continue for several repeat Δ30 nM of biotin-pep-BHQ-1. The samples were excited at 400 nm since BHQ-1 have minimal absorption at that wavelength so can avoid direct excitation of BHQ-1.

i) QDs selection: Spectral overlap integral and Förster radius calculation

Figure 4A describes the normalized absorption and emission spectra of

biotin-pep-BHQ-1 molecule QDs525, QDs565, QDs585, and QDs655 respectively. The spectral overlap integral and the Förster radius were calculated using the equation (6) and (4) respectively and are described in Figure 4B. The excellent overlap integral between QD585 and BHQ-1 molecule satisfies the FRET theory to accomplish excellent energy transfer between the two.

From Figure 5A and Figure 5B it could be observed that a monotonous decrease in the PL intensity of donor QD585 at each step titration with various concentration of acceptor biotin-pep-BHQ-1. The photographic image in Figure 5C shows the quenching of QD585 PL upon increasing the number of biotin-pep-BHQ-1 molecule per quantum dot.

b) Time resolved Photoluminescence measurement

Figure 6A describes the QD585 decay profile at various biotin-pep-BHQ-1 concentrations. PL decay curve were fitted with a third order exponential function, as it is masking a decay mechanism with more than three possible routes.

$$F(t) = \alpha_1 e^{-t\tau_1^{-1}} + \alpha_2 e^{-t\tau_2^{-1}} + \alpha_3 e^{-t\tau_3^{-1}} + C \qquad (12)$$

where F is the PL intensity, t is time, C is a constant, A_i is an amplitude, and τ_i is a lifetime component. Amplitude-weighted average lifetimes were calculated according to equation 13, assuming τ_{av} is the most appropriate quantity for analyzing FRET efficiency.

$$\tau_{av} = \frac{(\tau_1\alpha_1+\tau_2\alpha_2+\tau_3\alpha_3)}{(\alpha_1+\alpha_2+\alpha_3)} \qquad (13)$$

The time-resolved PL of the semiconductor quantum dot directly reflects the transient population that is distributed in the radiative core states. The heterogeneity in size, shape, degree of aggregation, surface passivation and structure within a given quantum

dot sample are causes for multiexponential dynamics of the excitonic decay of colloidal CdSe QDs.[92,93] It has been proved by Marcus *et al*. that the multiexponential function fit the data well compared to the stretched exponential function, hence pointed out the chance of existence of a number of discrete relaxation pathways with individual concomitant lifetime even though the exact number and identity of the pathways are unknown.[57] This heterogeneity leads to a variety of decay processes available to band-edge excitons, where each observed time constant, τ, is an average excited state lifetime for a population of QDs with a set of available decay pathways ranging in time scale from hundreds of femptosecond to microseconds.[94–97] In addition to radiative recombination, decay of the excited state population depends on several competing radiationless processes such as Auger relaxation of hot electrons, spin relaxation, phonon induced carrier relaxation, biexciton decay, carrier trapping at nanocrystal defects, charge transfer into ligand based orbital and relaxation to the ground state.

In the present case, the two decay constants shall be assigned to the Auger process and a combination of spin-allowed and forbidden relaxations when there is no energy transfer. Indeed, FRET or any other fast relaxation process suppresses the intrinsic slow radiative recombination processes. As a result, the fast process becomes clear during energy transfer, because the energy transfer competes with the relatively slow relaxations in the dark exciton state or surface states. The FRET efficiency of QD585-(pep-BHQ-1)$_n$ nanobioassembly at various concentration of acceptors are calculated using equation 8. Table 2 describes the determined FRET efficiency values. Figure 6B describes the wavelength dependent nanosecond PL decay profiles of QD585-(pep-BHQ-1)$_n$ nanobioassembly at various ratios from CCD detector of streak camera. Similar to the steady state PL intensity results, the average

exciton lifetime (τ_{av}) also decreases with increasing biotin-pep-BHQ-1 assembled per QD.

c) Stern-Volmer analysis

Figure 7 describes the apparent PL quenching ratio of QD in the absence and presence of biotin–pep-BHQ-1 during the QD-(pep-BHQ-1)$_n$ nanobioassembly formation. A careful evaluation of the graph plotted in Figure 7A proposes an inherent bimodal process with an inflection at an apparent ratio of 1: 40 QD and biotin-pep-BHQ-1 respectively. The linear fit shown in Figure 7B between biotin-pep-BHQ-1 concentration of 0 to 40 nM while that for subsequent n ≥ 40 to 130 biotin-pep-BHQ-1 closely resembles the linear quenching by only the BHQ-1 molecule. This would correspond to a highly initial rate of quenching expected for biotin-pep-BHQ-1 directly attached to the QD along with a subsequent much weaker, linear-quenching process driven by Stern-Volmer solution phase collisional quenching interactions. The Stern-Volmer constant was 1.7×10^7 M^{-1} based on the slope of a plot up to n~40; the apparent bimolecular quenching constant was equal to 1.6×10^{15} $M^{-1}s^{-1}$. The various reasons for a deviation from the theoretical value of streptavidin-biotin binding constant has been described extensively in previous studies.[98] It should be considered that the solid support for streptavidin-biotin interaction significantly affects the kinetics of the reaction due to the diffusion limitation and steric hindrance.[99] The steady state luminescence time evolution spectra of QD PL quenching upon titration with different concentration of biotin-pep-BHQ-1 was performed as shown in Figure 8; it is observed that as the concentration of biotin in solution increases the streptavidin-biotin binding rate also increases. Also, there is no evidence of any cooperative interaction between the biotin molecules on the surface of same particle

with streptavidin on its surface.[100] Hence, the lower concentration of biotin upon stoichiometric titration, QDs solid surface induced diffusion limitation and steric hindrance reduces the streptavidin-biotin binding reaction kinetic rates and shows deviation from the theoretically predicted value of the binding constant.

d) Evaluation of FRET efficiency

Peak emission intensities, were calculated from emission spectra by averaging the measured intensities within ±2 nm of the peak emission wavelength. Streptavidin-biotin mediated self-assembly of biotin-pep-BHQ-1 on QDs brings BHQ-1 acceptors in the close proximity of QD and results in efficient FRET. Such streptavidin-biotin mediated site-specific labeling of QDs provides a homogeneous donor to acceptor distances, while forming a concentric energy transfer system. The average energy transfer efficiency E is calculated from each set of donor-acceptor conjugates using the expression 8. FRET efficiency determined from the steady state PL measurement of QDs585-(pep-BHQ-1)$_n$ nanobioassembly were described in Table 1. Table 3 describes the estimated FRET efficiency values of QDs565-(pep-BHQ-1)$_n$ nanobioassemblies. Table 2 describes the calculated value of FRET efficiency from average life time values obtained from time–resolved experiment for each QDs585-(pep-BHQ-1)$_n$ nanobioassembly. In the current nanobioassembly configuration multiple numbers of BHQ-1 dyes can array on the QD surface in a concentric manner through the streptavidin-biotin-peptide bio bridge. This concentric array result in an equivalent enlargement of spectral overlap integral with increasing number of biotin-pep-BHQ-1, which proportionately increases the FRET efficiency compared to one QD-one BHQ-1 pair, this can also be called as FRET cross-section[101] enhancement with increasing number of BHQ-1 per QD.

Confirming the statement it is observed in Figure 5 that QD585 donor intensity is gradually monotonously reducing upon binding of increasing number of biotin-pep-BHQ-1 in the QD-(pep-BHQ-1)$_n$ nanobioassembly. Figure 11A describes the evaluated FRET efficiency of QD585-(pep-BHQ-1)$_n$ nanobioassembly with increasing biotin-pep-BHQ-1 molecule. The wavelength dependency of energy transfer rate describes that within a set of donors and acceptors, even though the number of donor and acceptor molecule are the same and are under the same experimental conditions susceptible to different FRET efficiencies because of the distinct differences in their spectral overlap.[102] A QDs sample is an ensemble of slightly different sizes of quantum dots hence the overall PL profile of an ensemble solution is contributed by the narrow emissions from each of these slightly different sized QDs.

The wavelength-dependency of PL quenching in a donor–acceptor system is a spectroscopic tool for confirming the FRET process, but its non existence could propose the possibility of other quenching processes. The validation of PL quenching wavelength dependency in this case was examined by designing an experiment with a fixed concentration of QDs having different photo emission maximum and with a fixed concentration of biotin-pep-BHQ-1 acceptors. That is a molar ratio of 1:40 kept for each reaction mixtures in order to make a QD-(pep-BHQ-1)$_{40}$ nanobioassembly. The PL quenching spectra of each nanobioassembly with various wavelength emissive QD donor and biotin-pep-BHQ-1 were described in Figure 9 and quenching efficiency of QD-(pep-BHQ-1)$_n$ nanobioassembly were plotted in Figure 10. Figure 11B quantitatively describes the equivalency between QD quenching efficiency derived from steady state PL intensity and time-resolved average decay life time data and hence express meaningful correlation with the equation 14.

$$E = 1 - \frac{F_{DA}}{F_D} = 1 - \frac{\tau_{DA}}{\tau_D} \quad (14)$$

2.5 Conclusion

A QD-(pep-BHQ-1)$_n$ nanobioassembly was successfully constructed with bridging QDs donors and BHQ-1 acceptors through a MMP-2 targeting PLGVR amino acid sequence containing short peptide. Steady state PL intensity measurement observed a monotonous decrease in the PL intensity of QD when assembled to different number of biotin-pep-BHQ-1. A similar monotonous reduction in PL decay life time also observed through time resolved experiments. The wavelength-dependency PL quenching process confirms the inherent FRET dynamics in the nanobioassembly. The comparison of calculated quenching efficiency values from steady state PL intensity and time-resolved average decay life time confirms the existence of FRET signal transduction channel in QD-(pep-BHQ-1)$_n$ nanobioassembly.

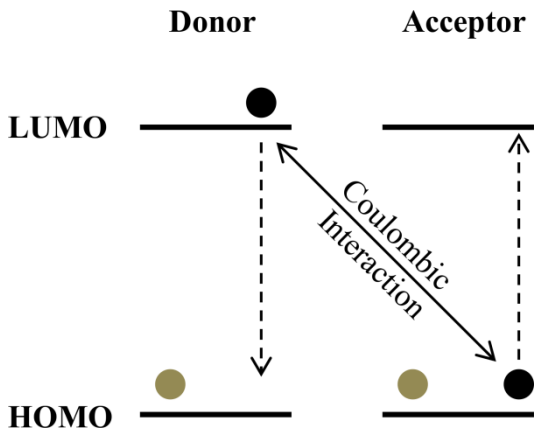

Figure 1. Förster Resonance Energy Transfer process. Excitation of the proximal acceptor molecule from HOMO (highest occupied molecular orbital) to LUMO (lowest unoccupied molecular orbital) is achieved by inducing an acceptor dipole oscillation through Coulombic interaction with the excited donor molecule.

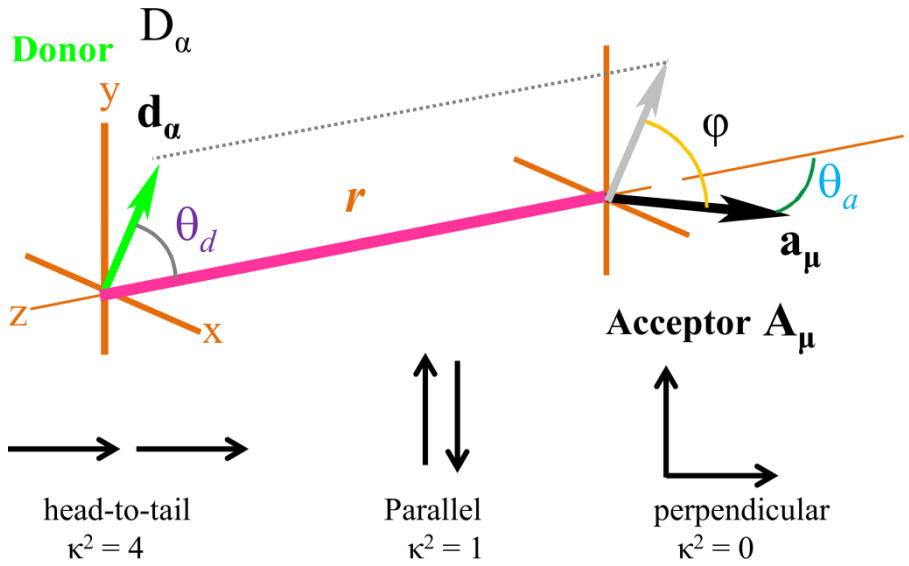

Figure 2. Schematics of mutual orientation of the α-th excited donor molecule emission transition dipole moment $(\vec{d}_\alpha)$ to μ-th acceptor absorption transition dipole moment $(\vec{a}_\mu)$ and the impact on κ^2.

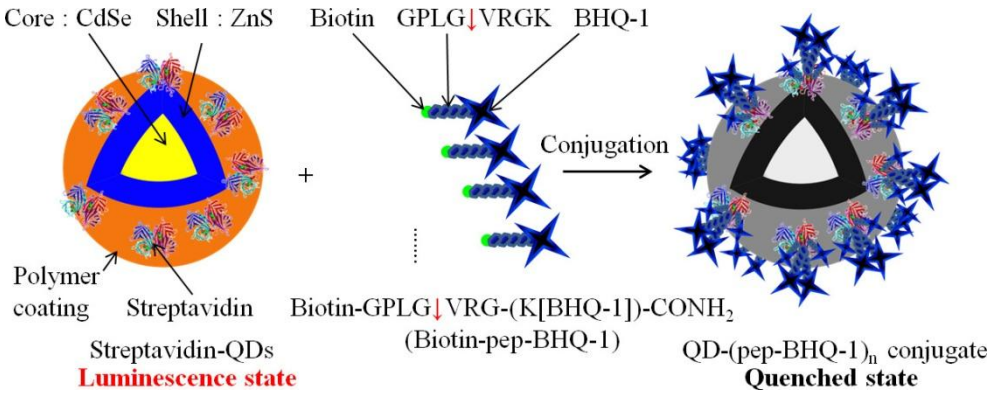

Figure 3. Schematic diagram of the quenching of quantum dot (QD) photoluminescence by using black hole quencher-1 (BHQ-1) molecules. This diagram shows that streptavidin-QDs585 nm are conjugated with biotin-Glycine-Proline -Leucine-Glycine-Valine-Arginine-(LysineBHQ-1)-amide,{(biotin-GPLGVRGK[BHQ-1])-$CONH_2$; biotin-pep-BHQ-1)} forms a QD-(pep-BHQ-1)$_n$ nanobioassembly and QD photoluminescence was quenched by BHQ-1 molecules.

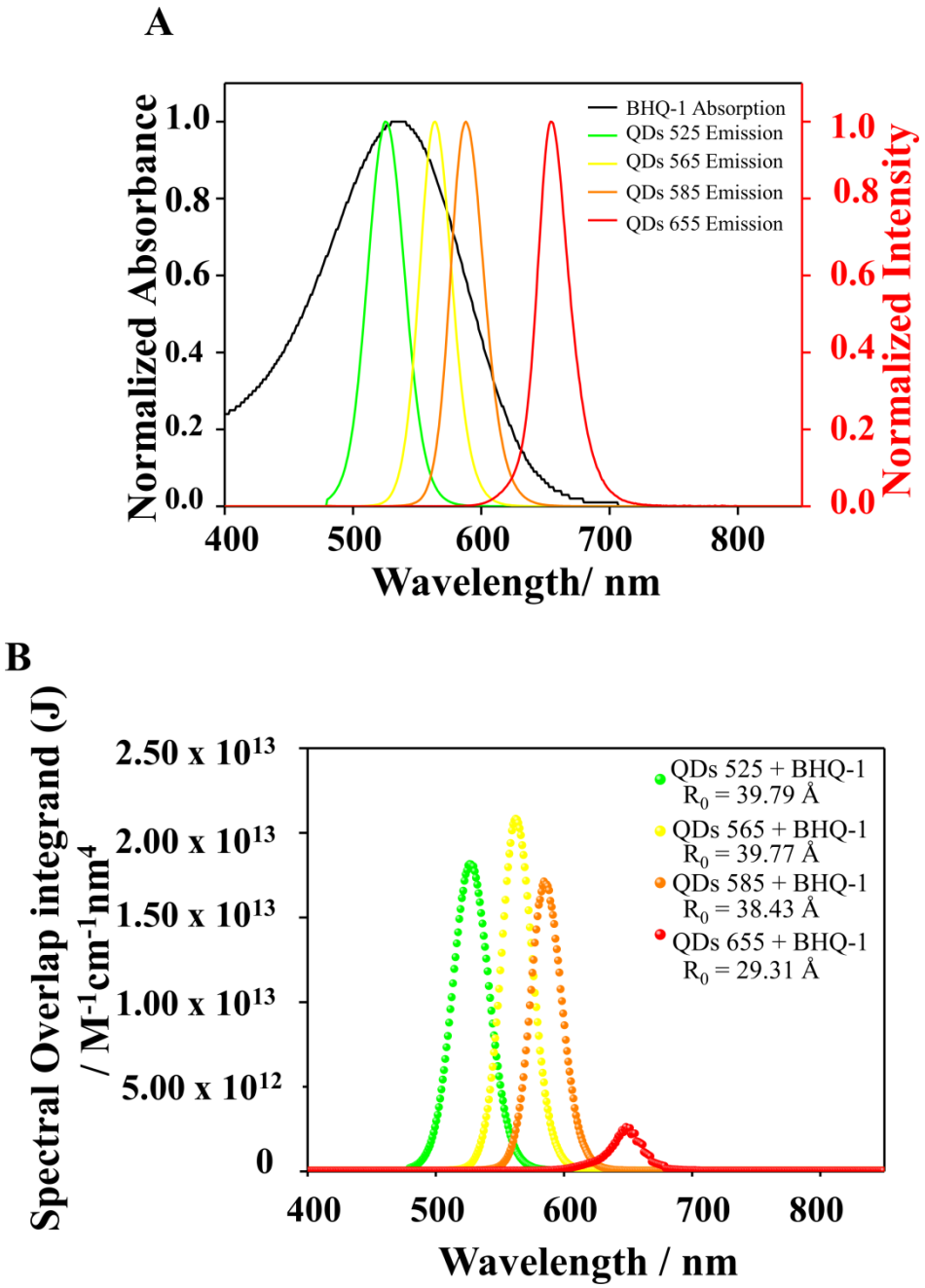

Figure 4. A. Normalized absorption spectra of biotin-pep-BHQ-1 molecule and normalized emission intensity of QDs525, QDs565, QDs585 and QDs655. B. The spectral overlap integral of various QDs donors and biotin-pep-BHQ-1 acceptor combinations, the Förster radius R_0 value for each donor- acceptor combinations has presented.

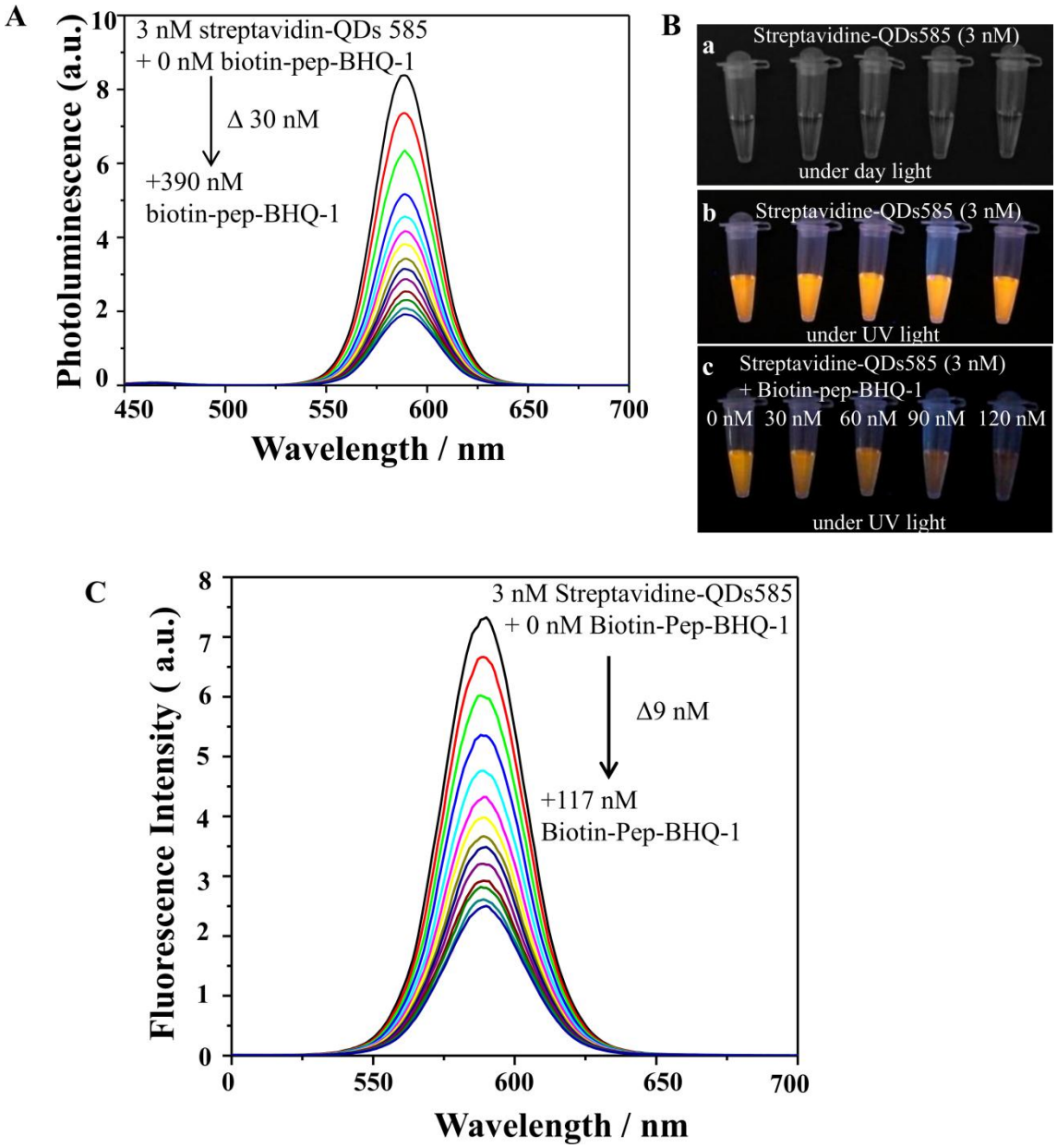

Figure 5. Evolution of the steady-state photoluminescence quenching spectra of streptavidin-QDs585 in the QD-pep-BHQ-1 nanobioassembly. 3 nM streptavidin-QDs585 was titrated against various concentrations of biotin-pep-BHQ-1, 0-390 nM in Milli-Q water. Samples were excited at 400 nm.

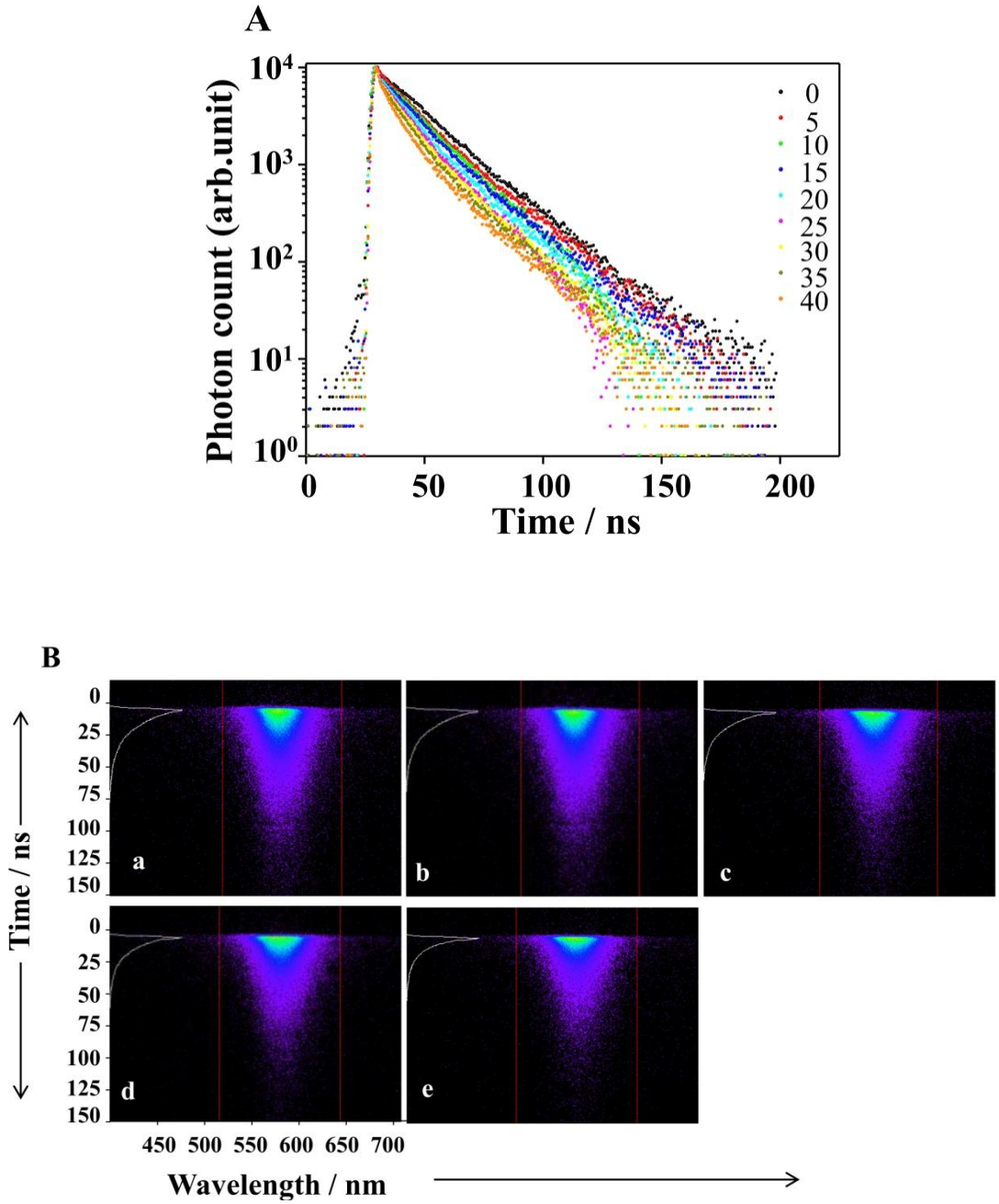

Figure 6. A. Time resolved excited state lifetime analysis of QD-(pep-BHQ-1)$_n$ nanobioassembly. Streptavidin-QD585 conjugated with the indicated increasing ratios of biotin-pep-BHQ-1. QD are excited at low absorption wavelength of BHQ-1 molecule at 400 nm using 150 fs laser pulses (6.3 W/cm^2). B. Nanosecond PL decay profiles of QD-(pep-BHQ-1)$_n$ conjugates recorded by the streak camera.

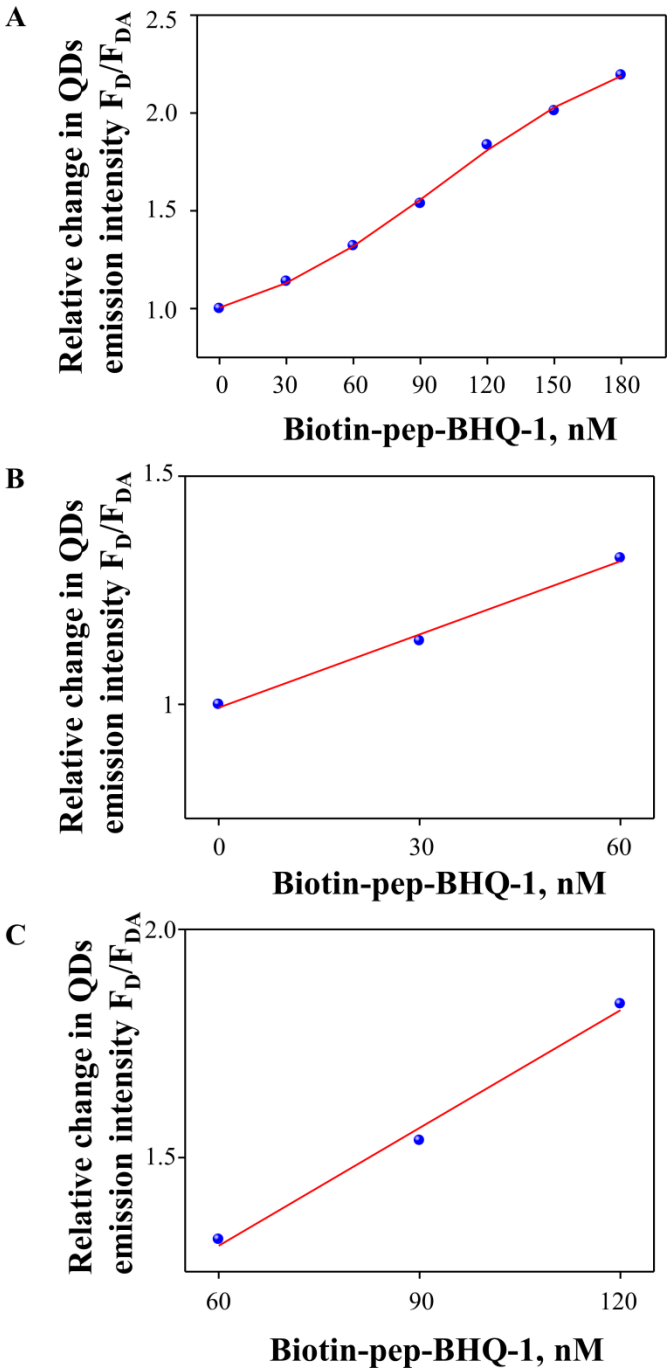

Figure 7. The relative change in the photoluminescence intensity (F_D/F_{DA}) of 3 nM QD585 (F_D) upon titration with biotin-pep-BHQ-1 (F_{DA}) were graphically represented as a Stern-Volmer plot. **A.** Stern-Volmer plot of 3 nM QD585 titrate with 0-180 nM biotin-pep-BHQ-1 molecule, sigmoidal fit of the data points are presented. **B** and **C.** Stern-Volmer plot of 3 nM QD585 titrate with 0-60 nM and 60-120 nM biotin-pep-BHQ-1 molecules respectively, linear fit of the data points are presented.

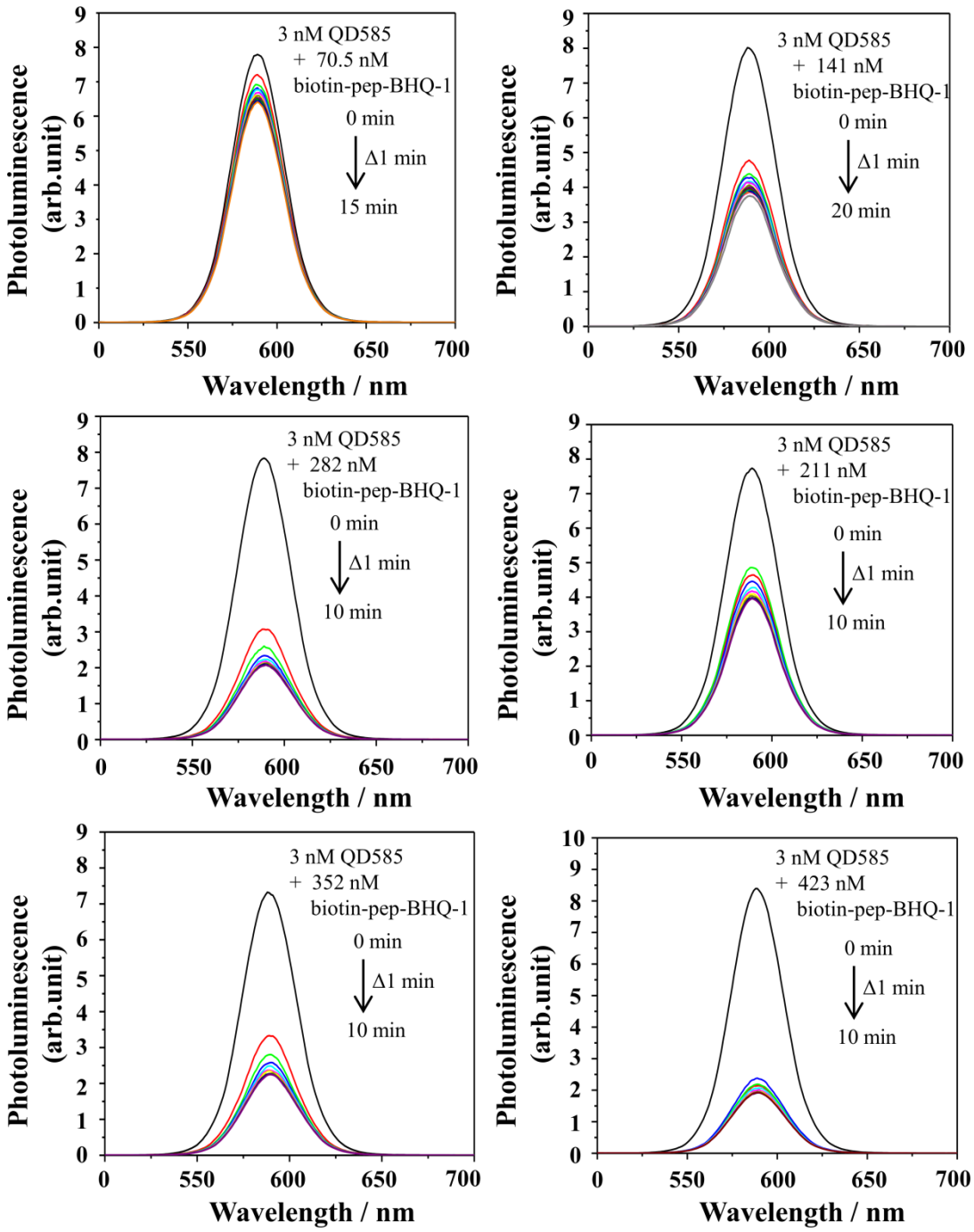

Figure 8. Temporal photoluminescence evolution of streptavidin-QD585 from the time of titration with various concentration of biotin-pep-BHQ-1 molecules.

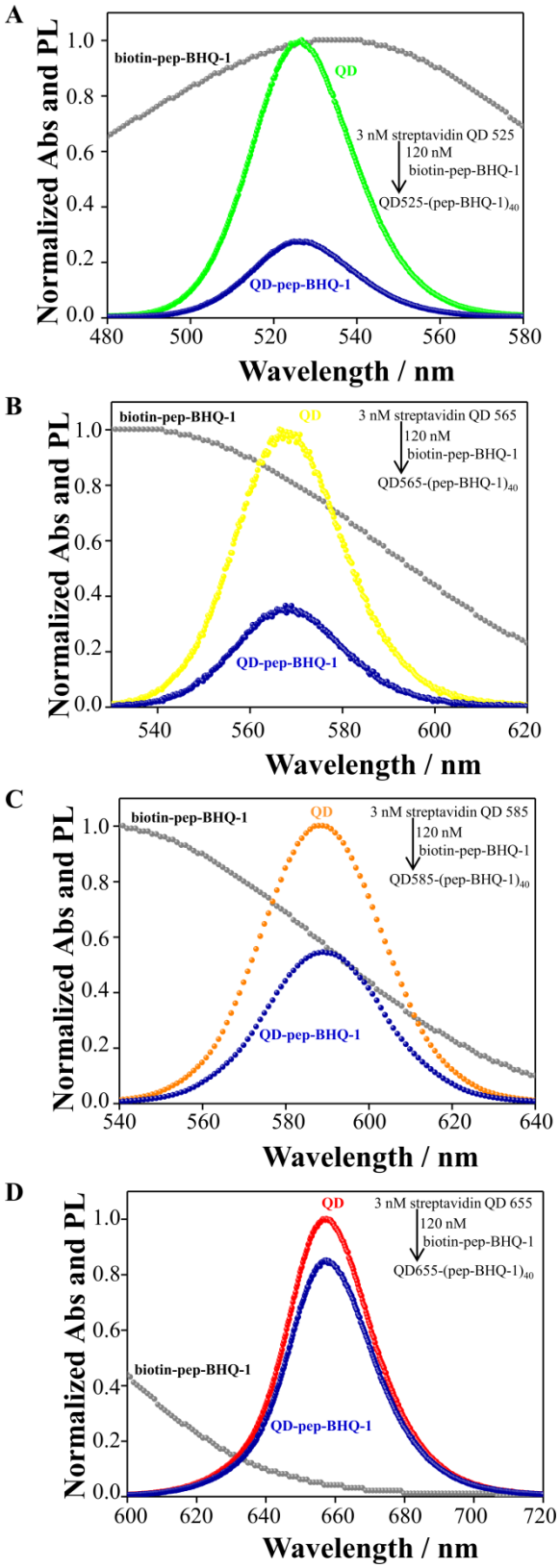

Figure 9. Wavelength dependent QDs PL quenching profiles. Photoluminescence

spectra of the (A) 525 nm, (B) 565 nm, (C) 585 nm and (D) 655 nm QDs alone and after assembled with 40-biotin-pep-BHQ-1 acceptors. Samples were excited at 400 nm.

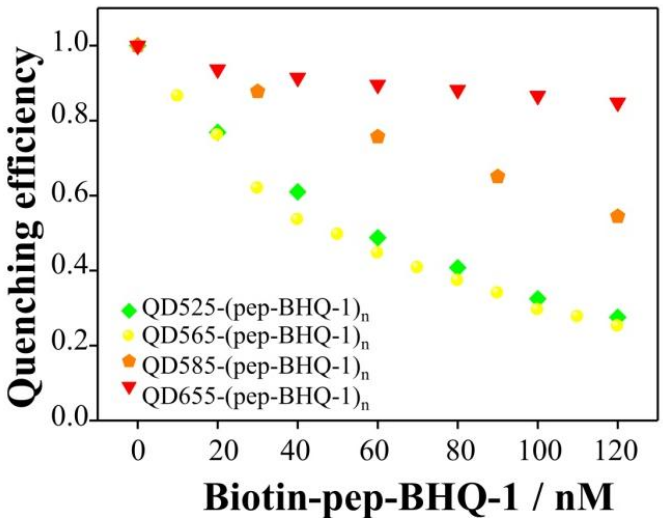

Figure 10. The quenching efficiency of various QD-(pep-BHQ-1)$_n$ nanoassemblies at a fixed biotin-pep-BHQ-1 acceptor concentration.

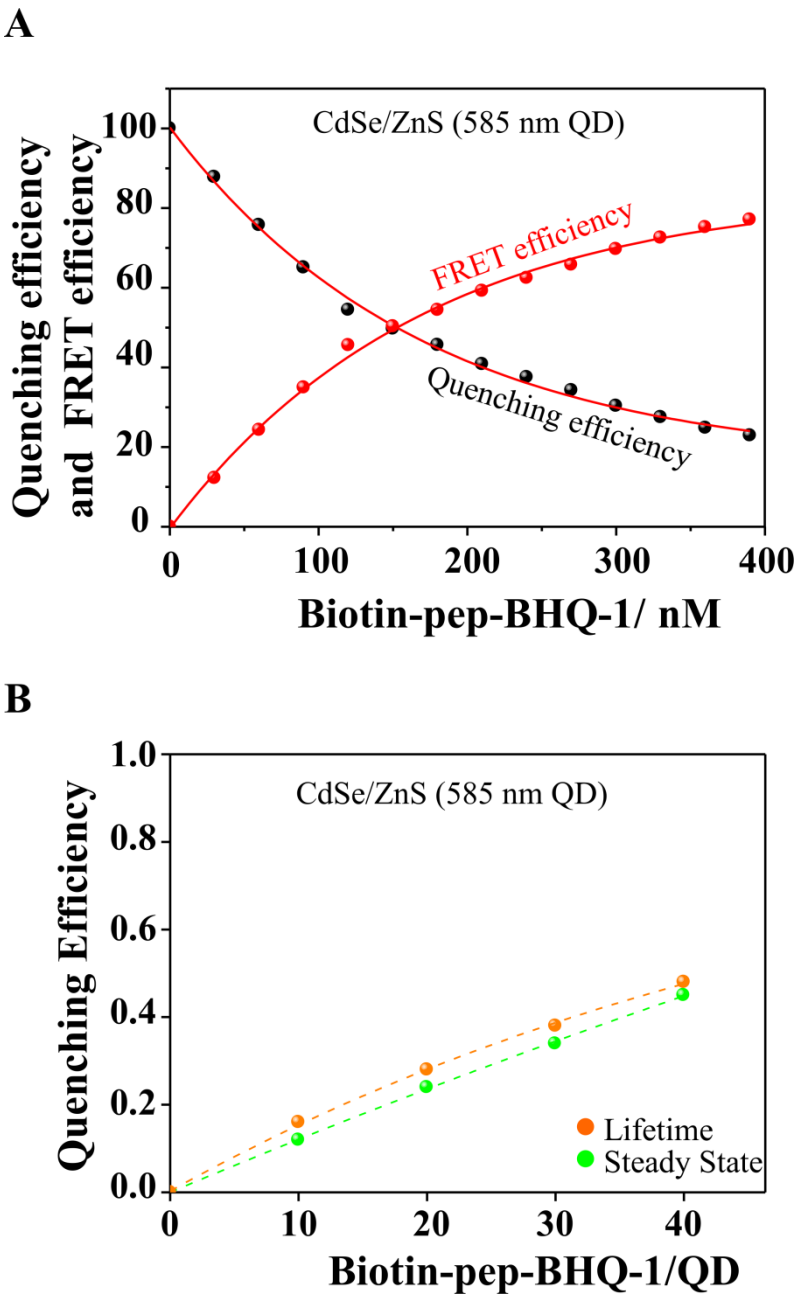

Figure 11. A. FRET efficiency data from QD-pep-BHQ-1 nanobioassembly. QD, PL quenching reported as a percentage in black and the corresponding FRET efficiency as a function of biotin-pep-BHQ-1 concentration titrating against 3 nM concentrations of streptavidin QD585 are presented in red. B. Comparison of normalized quenching profiles from steady-state versus time resolved PL decay data of QDs585 nm versus

increasing ratio of biotin-pep-BHQ-1 assembled per QD. Normalized steady state data are plotted in green while the corresponding time-resolved PL decay is shown in orange.

Table 1**.** QD585 steady state intensity ratio collected from QD-(pep-BHQ-1)$_n$ nanobioassembly.

Sample	**F_D/F_{DA}**	**PL Quenching (%) F_{DA}/F_D**	**FRET Efficiency (%) $E= 1- F_{DA}/F_D$**
3 nM QD585	1	1	0
3 nM QD585 + 30 nM biotin-pep-BHQ-1	1.14	87.78	12.22
3 nM QD585 + 60 nM biotin-pep-BHQ-1	1.32	75.71	24.29
3 nM QD585 + 90 nM biotin-pep-BHQ-1	1.62	61.67	38.33
3 nM QD585 + 120 nM biotin-pep-BHQ-1	1.84	54.44	45.56
3 nM QD585 + 150 nM biotin-pep-BHQ-1	2.01	49.71	50.29
3 nM QD585 + 180 nM biotin-pep-BHQ-1	2.19	45.58	54.42
3 nM QD585 + 210 nM biotin-pep-BHQ-1	2.45	40.79	59.21
3 nM QD585 + 240 nM biotin-pep-BHQ-1	2.66	37.55	62.45
3 nM QD585 + 270 nM biotin-pep-BHQ-1	2.92	34.24	65.76
3 nM QD585 + 300 nM biotin-pep-BHQ-1	3.30	30.29	69.71
3 nM QD585 + 330 nM biotin-pep-BHQ-1	3.64	27.46	72.54
3 nM QD585 + 360 nM biotin-pep-BHQ-1	4.03	24.81	75.19
3 nM QD585 + 390 nM biotin-pep-BHQ-1	4.37	22.90	77.10

Table 2**.** QD 585 average life time from time resolved experiment

Sample	**τ_{av} (ns)**	**$E = 1 - \tau_D / \tau_{DA}$**
3 nM QD585	10.03	0
QD585-(pep-BHQ-1)$_5$	8.96	0.10
QD585-(pep-BHQ-1)$_{10}$	8.35	0.17
QD585-(pep-BHQ-1)$_{15}$	7.91	0.21
QD585-(pep-BHQ-1)$_{20}$	7.16	0.29
QD585-(pep-BHQ-1)$_{25}$	6.66	0.34
QD585-(pep-BHQ-1)$_{30}$	6.18	0.38
QD585-(pep-BHQ-1)$_{35}$	5.78	0.42
QD585-(pep-BHQ-1)$_{40}$	5.15	0.49

Table 3. QD565 steady state intensity ratio collected from QD-(pep-BHQ-1)$_n$ nanobioassembly..

Sample	**F_D/F_{DA}**	**PL Quenching (%) F_{DA}/F_D**	**FRET Efficiency (%) E= 1- (F_{DA}/F_D)**
3 nM QD565	1	100	0
3 nM QD565 + 10 nM biotin-pep-BHQ-1	1.16	86.53	13.47
3 nM QD565 + 20 nM biotin-pep-BHQ-1	1.31	76.20	23.80
3 nM QD565 + 30 nM biotin-pep-BHQ-1	1.61	61.96	38.04
3 nM QD565 + 40 nM biotin-pep-BHQ-1	1.86	53.60	46.40
3 nM QD565 + 50 nM biotin-pep-BHQ-1	2.01	49.65	50.35
3 nM QD565 + 60 nM biotin-pep-BHQ-1	2.24	44.67	55.33
3 nM QD565 + 70 nM biotin-pep-BHQ-1	2.45	40.75	59.25
3 nM QD565 + 80 nM biotin-pep-BHQ-1	2.68	37.33	62.67
3 nM QD565 + 90 nM biotin-pep-BHQ-1	2.94	34.01	65.99
3 nM QD565 +100 nM biotin-pep-BHQ-1	3.39	29.55	70.45
3 nM QD565 +110 nM biotin-pep-BHQ-1	3.61	27.66	72.34
3 nM QD 565+120 nM biotin-pep-BHQ-1	3.97	25.18	74.82
3 nM QD565 +130 nM biotin-pep-BHQ-1	4.25	23.51	76.49
3 nM QD565 +140 nM biotin-pep-BHQ-1	4.66	21.48	78.52
3 nM QD565 +150 nM biotin-pep-BHQ-1	4.92	20.32	79.68
3 nM QD565 +160 nM biotin-pep-BHQ-1	5.49	18.22	81.78
3 nM QD565 +170 nM biotin-pep-BHQ-1	5.61	17.84	82.16
3 nM QD565 +180 nM biotin-pep-BHQ-1	6.28	15.92	84.08

Chapter 3. Quantum dot-peptide nanoassembly on mesoporous silica nanoparticle

3.1 Introduction

Mesoporous silica nanoparticle has been widely used as a functional entity in sensing, imaging, drug delivery and therapy due to the easiness and possibilities of various chemical modification and bioconjugation reaction at its surface.[103] Since the MMP2 are localized at the cancer cells surface due to the interaction with αvβ3 integrin receptors, we designed a new functional form of the nanoassembly through incorporating a 200 nm mesoporous silica nanoparticle scaffold keeping the aim of localization of MMP2 target peptide GPLG↓VRGK, the MSN scaffold is non fluorescent material and which can accommodate maximum number of MMP2 target peptide in a nano space volume, the large size of the MSN scaffold not only provide enough space for attaching suitable biological moieties for receptor targeted attachment but also inhibit itself from transduction into the cell, which is a specific need for cell surface sensors.

3.2 Materials

a) Donor

Streptavidin conjugated CdSe/ZnS QD having photoemission maximum at 525 nm (QD525) Life Technologies (Tokyo, Japan). A 3 nM sample of QD525 has made with milli-Q water (Millipore Milli-Q Lab purification system, Tokyo, Japan).

b) Acceptor

A peptide of the form biotin-GPLG↓VRG(Lys[BHQ-1])-$CONH_2$, with 99% purity was

designed and custom made from Custom Peptide & Antibody Service, Eurofins Genomics K.K. (Tokyo, Japan). The peptide contains PLGVR amino acid sequence which functions as MMP-2 target. 1 mM sample of biotin-pep-BHQ-1 has made in DMSO and diluted further in other medium with respect to the experiments

c) Scaffold material and reagent

Mesoporous silica nanoparticle 200 nm were purchased from Sigma Aldrich, Tokyo, Japan. Sulfo- NHS-Biotin, EZ-Link purchased from Thermo Fisher Scientific, (Tokyo, Japan). (3-aminopropyl) triethoxysilane (APTES) purchased from Sigma-Aldrich, (Tokyo, Japan).

3.3 Methods

a) Bioconjugation of QD-(pep-BHQ-1)$_n$ to mesoporous silica nanoparticles.

Figure 12B shows the schematics of conjugation of QD525 and biotin-GPLG↓VRG(Lys[BHQ-1])-$CONH_2$ and its conjugation to mesoporous silica nanoparticle surface. 1 mg of 200 nm silica nanoparticle powder sample dispersed in 0.95 mL of acetone. 50 μL of 1% APTES in acetone solution was added to the above dispersion and mixed well for 1 hour at room temperature, repeatedly washed with acetone and collected by centrifugation. Successively, 1 mL of 2.25 mM sulfo-NHS-biotin solution in milli Q purified water were added to the former sample, mixed well for 1 hour, washed with Milli-Q water five times and dispersed in 1 mL of Milli-Q water. Next, 50 nM QD525 solution was added to the dispersion, mixed well for 30 min, washed with water several times, collected by centrifugation and dispersed in 1 mL Milli-Q water. Finally, 1.5 μL of 1 mM biotin-pep-BHQ-1 solution was added to the above sample, mixed well for 30 min, washed five times with Milli-Q water, collected

by centrifugation and dispersed in 1 mL of Milli-Q water for measurement.

b)Transmission electron microscope

The samples were absorbed to carbon-coated copper grids (400 mesh). The grid were observed by a transmission electron microscope (JEM-1400 Plus; JEOL Ltd., Tokyo, Japan) at an acceleration voltage of 80 kV. Digital images (3296×2472 pixels) were taken with a CCD camera (EM-14830RUBY2; JEOL Ltd., Tokyo, Japan).

c) Steady state photoluminescence spectroscopy

Steady state PL spectral analysis of QD525 and QD-pep-BHQ-1 were performed by using a Fluorolog 3 (Horiba, Tokyo, Japan) Spectrofluorometer. QDs were excited at 400 nm to minimize direct excitation of BHQ-1.

d) Time-resolved photoluminescence spectroscopy

A 800 nm wavelength laser pulses from a regenerative amplifier (Reg A 9000, Coherent, Japan) seeded by a mode locked Ti: sapphire laser (Mira 900F, Coherent) pumped to optical parametric amplifier (OPA) (OPA 9400, Coherent Japan) and the second-harmonic generation (SHG) crystal in it generate a 400 nm wavelength laser pulses to excite the QD samples. QDs525 photoemission collected with an appropriate band-pass filter and directed to the entrance slit of the polychromator. An arrangement of a polychromator (250IS, Chromex, Japan) and a photon counting streak-camera (C4334, Hamamatsu, Japan) were used to record time resolved PL decay lifetime of QDs525.

3.3. Results and Discussion

a) TEM measurement

Figure13 describes the TEM images of the samples. Figure 13A shows the TEM

images of Mesoporous silica nanoparticle (MSN) and Figure 13B for MSN-[QD-(pep-BHQ-1)$_{30}$]$_{50}$ nanobioassembly.

b) Steady state FRET Measurement

The absorption spectrum of biotin-pep-BHQ-1 molecule, which is the energy acceptor, and the normalized PL spectra of CdSe/ZnS QD525, which is the energy donor, are shown in Figure 14 A, clearly showing significant spectral overlap between the two. Figure 12A shows graphical representation of QD525-pep-BHQ-1 conjugation procedure. Ratiometric amount of biotin-pep-BHQ-1 molecule was titrated against 3 nM QD525 solution. As prepared biotin-pep-BHQ-1 sample (2 μM) was added in each step of titration against a QD525 (3 nM, 200 μL). The titration procedure continued up to nine steps of repeated addition of biotin-pep-BHQ-1 and finally reached to a concentration of 180 nM. The resultant final QD-(pep-BHQ-1) conjugates has a ratio of 3:180, which is ~1:60. Thus, at each steps of titration, it is possible to calculate the apparent QD-pep-BHQ-1 conjugation ratios.

Addition of biotin-pep-BHQ-1 to a solution of streptavidin-functionalized colloidal QDs results in monotonous decrease of QD PL, which is attributed to conjugation of biotin-pep-BHQ-1 to QD, this self-assembly brings BHQ-1 acceptors in the close proximity of QD and subsequently FRET occurs from QD to BHQ-1. Streptavidin-biotin mediated self-assembly provides a thermodynamically probable homogeneous distribution of BHQ-1 on the surface of each QD, which results a QD-(pep-BHQ-1)$_n$ concentric energy transfer system. Assignment of QD PL quenching by BHQ-1 molecule to FRET is substantiated by the estimation of FRET efficiency. Emission intensities maxima were calculated by averaging the measured intensities within ±2 nm of the peak PL emission wavelength. The average energy

transfer efficiency E is calculated using the expression 8.

The spectral overlap integral between QD525 donor and BHQ-1acceptor conjugated on the surface mesoporous silica nanoparticle is shown in Figure 14B. The calculated spectral overlap integral *J* is ca 6.52×10^{14} $M^{-1}cm^{-1}$ and the Förster radius R_0 is ca 37.62 Å. Here the orientation factor $\kappa^2 = 2/3$ for freely rotating molecule. The quantum dots are conjugated to the mesoporous silica nanoparticle scaffold. But the QD molecule can rotate around along the streptavidin-biotin axis. The same way acceptor dipole can also rotate around each of the donor QD dipole as it is conjugated through streptavidin-biotin binding interaction. By increasing the number of energy acceptors per QD, we increase the effective acceptor extinction coefficient, which in turn proportionally improves the effective spectral overlap integral for single QD-multiple biotin-pep-BHQ-1 complexes.

Figure 15A describes the steady state PL spectra of titration experiment which shows the monotonous decrease in the PL intensity of a QD solution with increase in the concentration of biotin-pep-BHQ-1 conjugates, which indicates an increase in the number of biotin-pep-BHQ-1 molecules tethered to QD surface. Such a PL quenching indicates multiple, free biotin binding pockets on streptavidin-functionalized QDs. The PL intensity ratios (F_{DA}/F_D) in the titration results, which is the quenching efficiency acquired at each step of titration are indicated in Figure 15B (dark trace). The reciprocal of relative PL intensity ratios (F_D/F_{DA}) are plotted as a function of concentration of biotin-pep-BHQ-1, which helps us to extract quantitative information about PL quenching using a Stern-Volmer plot as shown in Figure 16; where F_{DA} is the PL intensity of QD in presence of biotin-pep-BHQ-1 molecules at each step of titration against 3 nM QD525 and F_D is the PL intensity of pristine QD525 acquired before

titration. A complex bimodal decay profile for QD PL was observed with increasing ratios of biotin-pep-BHQ-1 per QD. At a titration ratio of 180 nM biotin-pep-BHQ-1 per 3 nM QDs (1:60 molar ratio), ca 80% of QD PL has quenched, leaving ca 20% QD intact by BHQ-1. From information provided by the manufacturer, each QD are tethered with 5-10 streptavidin molecules. There will be maximum 4 free biotin binding pockets available per streptavidin, suggesting that each QD conjugate carries a maximum of 40 biotin-pep-BHQ-1 molecules. From the Stern-Volmer plot in Figure 16, observed a continuous and dynamic quenching process across all the concentrations of biotin-pep-BHQ-1 titrated against a 3 nM QD solution.

To obtain a clear picture of PL quenching, systematically analyzed the Stern-Volmer plot for a wide range of concentrations of biotin-pep-BHQ-1 as shown in Figure 16. Overall data in Figure 16A shows contributions of both dynamic and static quenching components. It is assumed that the excellent spectral overlap integral between QD525 emission and BHQ-1 absorption allows biotin-pep-BHQ-1 molecule to efficiently quench the QD emission through energy transfer process. The FRET efficiency of the QD-pep-BHQ-1 system was calculated using equation 8, and is plotted as a function of concentration of acceptor molecule at each step of titration, presented in Figure 15B, and the data points were analyzed with sigmoid fit. Figure 16B shows the graph plotting the slope of each data point in Figure 16A with the concentration of acceptor molecules. The graph shows maxima at a concentration of ≅80 nM. This shows that the quenching profile has an inflexion around 80 nM biotin-pep-BHQ-1. So here the SV plot needs two different plot fitted with two different equations before and after the inflexion points. From 0-80 nM was fitted using a quadratic equation as it contains both static and dynamic factors. The characteristic feature of Stern-Volmer

plots in such circumstances is an upward curvature, concave towards the y-axis as shown in Figure 16C. Then the fractional PL remaining F_{DA}/F_D is given by the product of fraction not complexed and the fraction not quenched by collisional encounters.[89]

$$\frac{F_{DA}}{F_D} = (1 + K_D[Q])(1 + K_s[Q]) \quad (15)$$

Here K_D and K_S are the dynamic and static Stern-Volmer constants. In order to calculate the K_D, K_S values, a graph has plotted taking $\left[\frac{F_{DA}}{F_D} - 1\right]$ along y-axix and [Q] along x-axis for the lowest three concentration, (20-60 nM biotin-pep-BHQ-1).

The value of $, K_S \cong 1.372 \text{x} 10^7$ M^{-1} and $K_D \cong 0$. The bimolecular quenching constant $k_q \cong 1.849\text{x}10^{15}$ $M^{-1}s^{-1}$. The bimolecular quenching constant k_q reflects the efficiency of quenching or the accessibility of fluorophore to the quencher. Diffusion controlled quenching typically results values of k_q near $1\text{x}10^{10}$ $M^{-1}s^{-1}$. Values of k_q larger than the diffusion-controlled limit usually indicate some type of binding interaction. Hence it is clear that there is a significant streptavidin-biotin interaction took place even at the lower concentration of initial titration experiments and resulted efficient QD PL quenching.

But after the inflexion point the Stern-Volmer plot shows a down-ward curvature that may be due to the presence of accessible and inaccessible or buried population of biotin-pep-BHQ-1 acceptor molecule. From 80-180 nM was fitted using a rational equation of the form $y = \frac{b+cx}{1+ax}$ where a,b,c are constant, which is similar to the following equation , as shown in Figure 16D.

The total fluorescence in the absence of quencher (F_0) is given by[89]

$$F = F_{0a} + F_{0b} \quad (16)$$

$$\Delta F = F_D - F_{DA} = F_{0a}\left(\frac{K_a[Q]}{1+K_a[Q]}\right) \quad (17)$$

$$\frac{F_0}{\Delta F} = \frac{1}{f_a K_a[Q]} + \frac{1}{f_a} \quad (18)$$

Where f_a is the fraction of initial fluorescence that is accessible to quencher.

$$f_a = \frac{F_{0a}}{F_{0b}+F_{0a}} \quad (19)$$

Where K_a is the Stern-Volmer quenching constant of the accessible fraction. To calculate the f_a and $K_a$values, a graph has plotted taking $F_D/\Delta F$ versus 1/[Q] for the highest three concentration, (140-180 nM biotin-pep-BHQ-1).

The calculated values of, $f_a = 0.9207$ and $K_a = 2.804\text{x}10^7$ M^{-1}

From the analysis it is clear that the static quenching factor is predominant throughout the titration experiments though the presence of slight dynamic quenching factors.

c) Time resolved FRET measurement

Here designed a new nanoassembly by incorporating a mesoporous nanoparticle (MSN) scaffold. The QDs-(pep-BHQ-1)$_n$ conjugates were arrayed on 200 nm MSN through streptavidin-biotin conjugation method. The advantages of MSNs are its simple separation after conjugate preparation, surface modification and other solution-based treatment process, which are owing to its high density (1.96 g/cm^3) when compared with polymer nanoparticles. Furthermore, MSNs are hydrophilic, biocompatible and

do not swell, which make them drug carriers and imaging probe for theranostics applications. After surface functionalization of MSN using APTES, a large number of biotin moieties were tethered to the surface of MSN by reacting with Biotin-sulfo-NHS ester, which was followed by conjugation of streptavidin QDs. An apparent ratio of 1:50 between MSN to QDs was maintained by adding 50 nM of QDs to the biotinylated MSN, which provided MSN-$(QD)_{50}$ conjugate. Similar procedure was followed in the preparation of MSN-$[QD\text{-}(pep\text{-}BHQ\text{-}1)_{30}]_{50}$ by treating biotin-pep-BHQ-1 with MSN-$(QD)_{50}$, which carries an apparent ratio of MSN (1) :QD (50) :biotin-pep-BHQ-1 (1500). Because of the high specific gravity of MSN, the conjugates gradually settle down during measurements in solution phase, which prevented us from obtaining steady-state PL intensity with accuracy. Therefore, FRET efficiencies were estimated by time-resolved PL measurement of MSN-$(QD)_{50}$ and MSN-$[QD\text{-}(pep\text{-}BHQ\text{-}1)_{30}]_{50}$ nanobioassembly.

Table 4 describes the individual decay component and average life time of QD525 in MSN-$(QD525)_N$ and MSN-$[QD\text{-}(pep\text{-}BHQ\text{-}1)_n]_N$ nanobioassembly. By considering the multiexponential nature of PL decay kinetics, we estimated average PL lifetime (τ_{av}) of MSN-$\{QD\text{-}(pep\text{-}BHQ\text{-}1)_{30}\}_{50}$ nanobioassembly at 5.22 ns. On the other hand, the average PL lifetime of QD on MSN scaffold but without biotin-pep-BHQ-1 is 13.90 ns. PL decay traces of QDs in MSN-$(QD)_{50}$ and MSN-$[QD\text{-}(pep\text{-}BHQ\text{-}1)_{30}]_{50}$ nanoassemblies are shown in Figure 17B, and the corresponding spectrally-resolved PL decay vs photocounts are shown in Figure 17C. Here, the short components of decays shall be assigned to Auger process and a combination of spin allowed and forbidden relaxations when there is no energy transfer. FRET suppresses intrinsic slow radiative relaxation processes. As a result, the fast process dominates during energy transfer.

MSN plays a key role in avoiding dynamic quenching due to non conjugated biotin-pep-BHQ-1 molecule, which became possible by removing freely diffusing biotin-pep-BHQ-1 molecules by centrifugation during sample preparation.

According to Förster theory and previous reports, FRET is significant only when the energy donor and proximal acceptor are within 100 Å. QDs involved in the current work have large hydrodynamic size (> 150 Å), according to the information provided by the manufacturer. The large size is contributed by ZnS shells, protective polymer layers, and streptavidin linkers. Therefore, it is likely that some QDs don't take part in FRET in the initial ratio metric titration of ensemble measurements. There are controversial reports on energy transfer between smaller and larger QDs.[104] Conversely Zheng *et al*. observed FRET channels in densely packed thin films of various sized CdSe QDs with the aid of ultrafast transient absorption spectroscopy where the separation between QDs are smaller than the size of the QDs and hence proves that the point- dipole approximation cannot any more gives quantitative information of FRET process in such cases.[105] In the current work, the average radius of QD is ≥ 75 Å, also, QDs are not directly conjugated to one another. Thus, rule out the possibility of QD to QD energy transfer. Biju *et al.* proves that there is no possible energy transfer induced PL quenching between two types QDs with size ≥ 75 Å.[106] Hence quenching of PL intensity and decrease of PL lifetime upon conjugation of pep-BHQ-1 to QD are contributed purely by QD to BHQ-1 energy transfer.

d) Simulation to calculate the approximate distance between QD andBHQ-1 .

The approximate distance between the QD and BHQ-1 molecule has evaluated as 62.57 Å(≅ 63 Å) using UCSF Chimera molecular modeling software as shown in Figure 18. This value can be taken as the approximate distance between QD and BHQ-1 molecule.

The separate calculation of the length of streptavidin as well as GPLGVRGK peptide has also calculated. The length of streptavidin is ≅ 50 Å and for GPLGVRGK peptide is ≅ 30 Å. So in total it will be ≅ 80 Å. But when biotin is conjugated to the specific site of streptavidin the length will get shortened as shown in the extended position model. So approximate distance between the QD and BHQ-1 (shown as small black sphere) molecule will be ≅ 63 Å, and which can vary depending on the rotation of streptavidin molecule. The modeling was done using UCSF Chimera molecular modeling software.

e) **Evaluation of FRET efficiency**

The FRET efficiency has calculated using the equation 7 and plotted in Figure 15B for each apparent ratio of QD-pep-BHQ-1 nanobioassembly. By applying average PL lifetime values in equation 8, the FRET efficiencies of MSN-{QD-(pep-BHQ-1)$_{30}$}$_{50}$ nanobioassembly estimated to be 62%, which is comparable to the steady state FRET efficiency of QD-(pep-BHQ-1)$_{30}$ nanobioassembly. The energy tansfer rate has calculated using the equation 3 and is equal to 4.76×10^6 s^{-1} as shown in Figure 14C and Figure 14D for both QD-(pep-BHQ-1)$_n$ and MSN-{QD-(pep-BHQ-1)$_n$}$_N$ nanobioassemblies.

3.4 Conclusion

In summary, the current work demonstrates ratiometric conjugation of BHQ-1-labeled MMP target peptide to QD and preparation of QD-(pep-BHQ-1)$_n$ nanobioassembly, this conjugate was further ratiometrically arrayed on mesoporous silica nanoparticles and synthesized MSN-{QD-(pep-BHQ-1)$_n$}$_N$ nanobioassembly in order to localize maximum PLGVR containing target peptide into a nanospace volume. The PL quenching of QDs in these assemblies was studied using steady-state and time-resolved

PL measurement. We observed considerable quenching of the PL intensity and decrease of PL lifetime of QDs when conjugated to multiple biotin-pep-BHQ-1 at each step of measurement over ratio metric titration. We attributed such PL changes to FRET from QD to proximal biotin-pep-BHQ-1 molecules. Nonetheless, we do not completely rule out a possibility that variations in the donor-to-acceptor center-to-center distance due to conformational dynamics of the linker peptide contribute to the experimental FRET efficiencies.

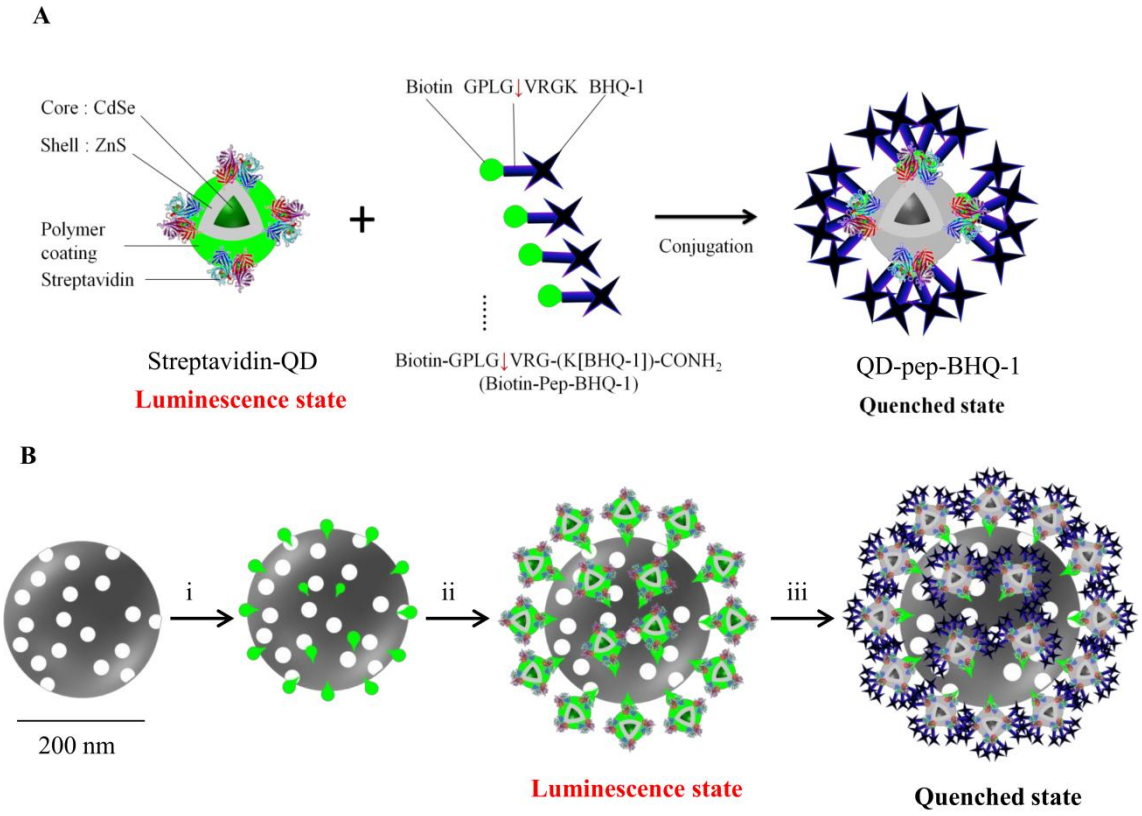

Figure 12. Scheme of preparation of donor-peptide-acceptor nanoassemblies, quenching of PL intensity of QD by energy transfer to BHQ-1 molecules and TEM images of nanoassemblies: (A) shows conjugation of streptavidin-QD525 with biotin-Glycine-Proline-Leucine-Glycine-Valine-Arginine-(Lysine-BHQ-1)-$CONH_2$; {(biotin-GPLG↓VRG(K[BHQ-1])-$CONH_2$; biotin-pep-BHQ-1)}, and QD photoluminescence is quenched by BHQ-1 molecules. (B). (i) Functionalization of mesoporous silica nanoparticle with primary amine using APTES, and biotinylation of the amino groups using Sulfo-NHS-Biotin, (ii) conjugation of QDs to silica nanoparticles, and (iii) conjugation of biotin-GPLGVRG(K-[BHQ-1])-$CONH_2$ to QDs tethered on silica nanoparticles.

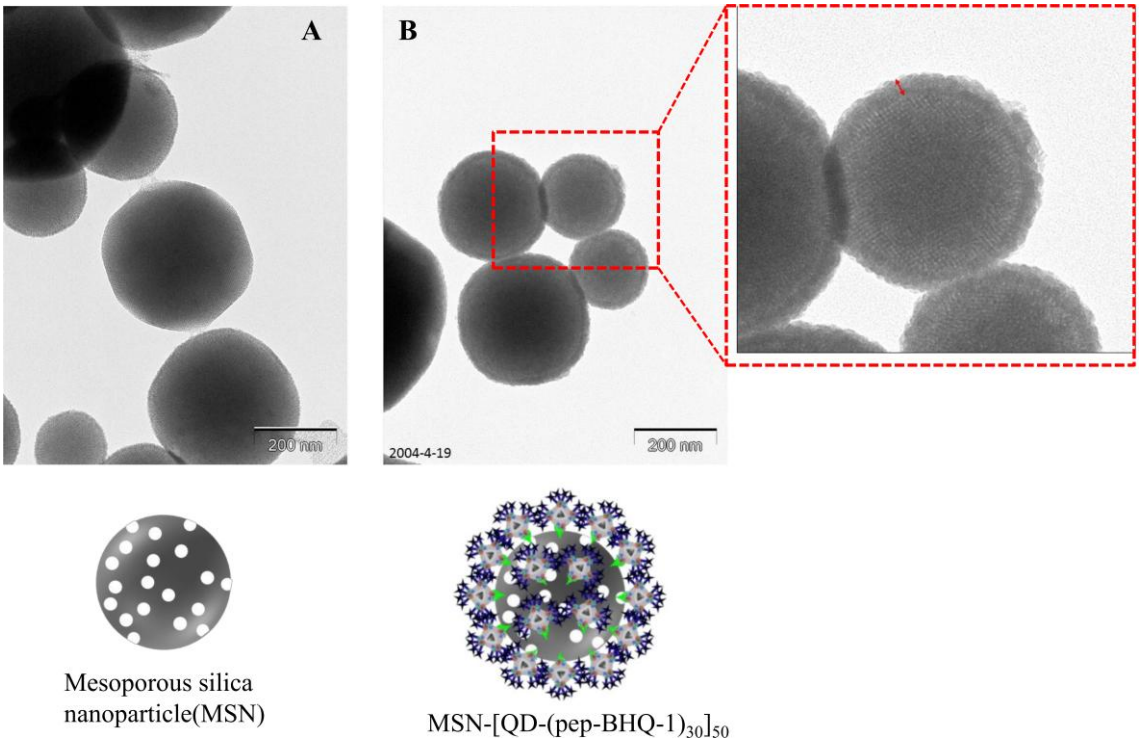

Figure 13. TEM images of (A) Mesoporous silica nanoparticle (MSN) and (B). MSN-[QD-(pep-BHQ-1)$_{30}$]$_{50}$ nanobioassembly.

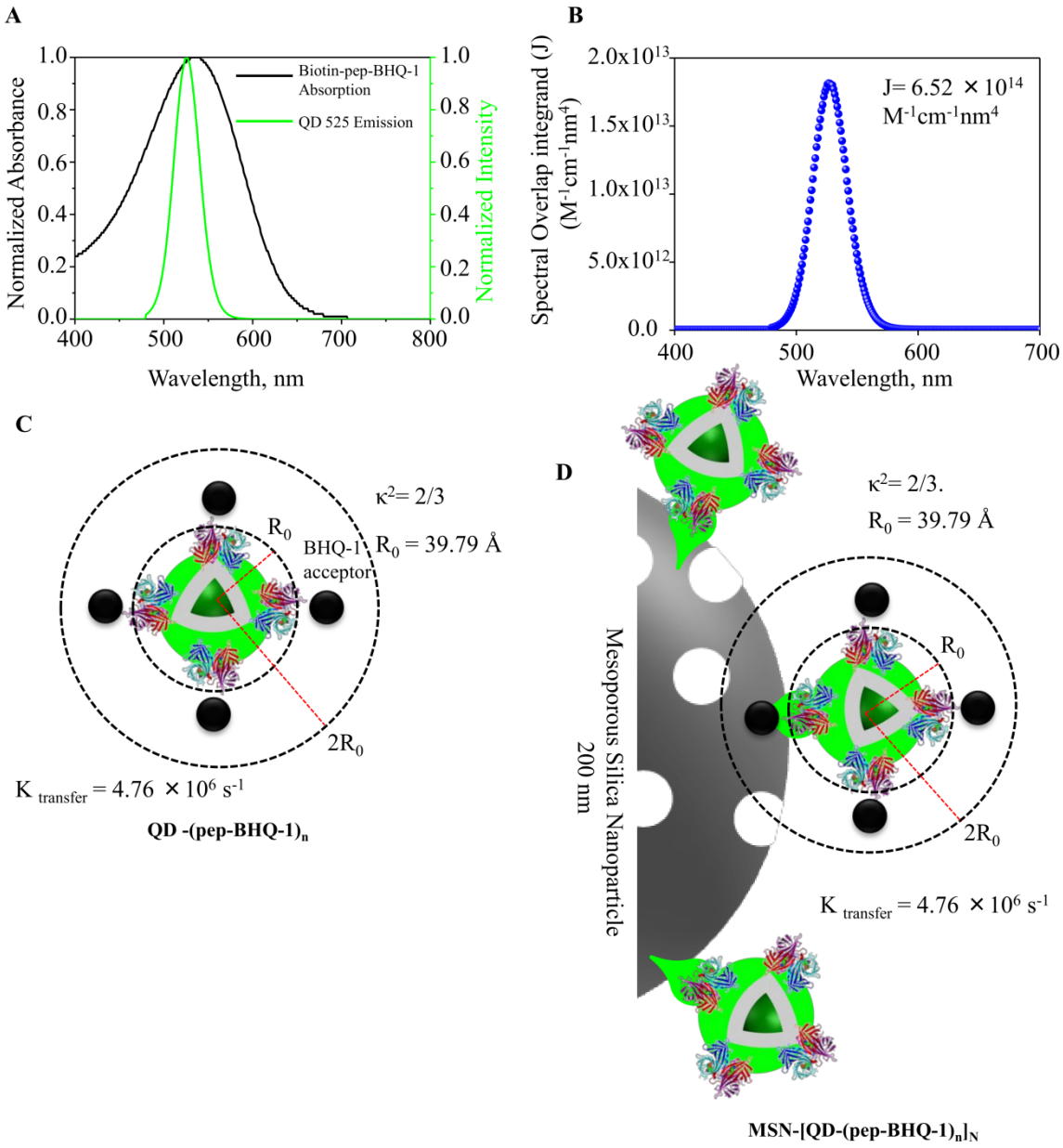

Figure 14. Steady state spectral characteristics (A) Normalized absorption and emission spectra of Black hole quencher -1 and QD525 respectively. (B) Estimated spectral overlap integral of QD525-pep-BHQ-1 conjugates.(C) & (D) Schematics to represent variation in R_0 values corresponding to the variation in dipole orientation factor value, κ^2= 2/3 for freely rotating molecule QD-(pep-BHQ-1)$_n$. But in MSN-[QD-(pep-BHQ-1)$_n$]$_N$ nanoassembly as well the acceptor molecule can freely rotate around the QD donor material since it bounding each other through streptavidin-biotin interaction, hence here also κ^2 value presumed to be 2/3 same as the former one.

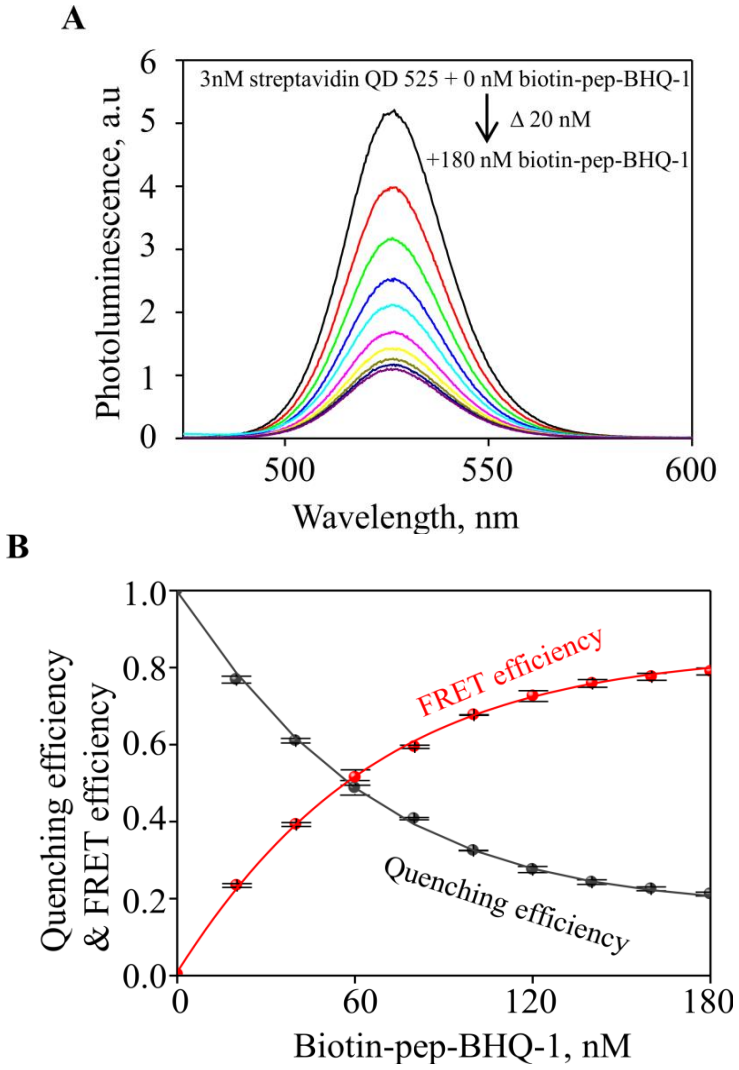

Figure 15. **A.** Evolution of the steady-state photoluminescence quenching spectra of QD525 in the QD-(pep-BHQ-1)$_n$ conjugates. 3 nM QD525 were titrated against various concentrations of biotin-pep-BHQ-1, 0-180 nM in purified water. Samples were excited at 400 nm. **B.** FRET efficiency data from QD-pep-BHQ-1 conjugates. QD, PL quenching reported as a percentage in black and the corresponding FRET efficiency as a function of biotin-pep-BHQ-1 concentration titrating against 3 nM concentrations of streptavidin- QD525 are presented in red.

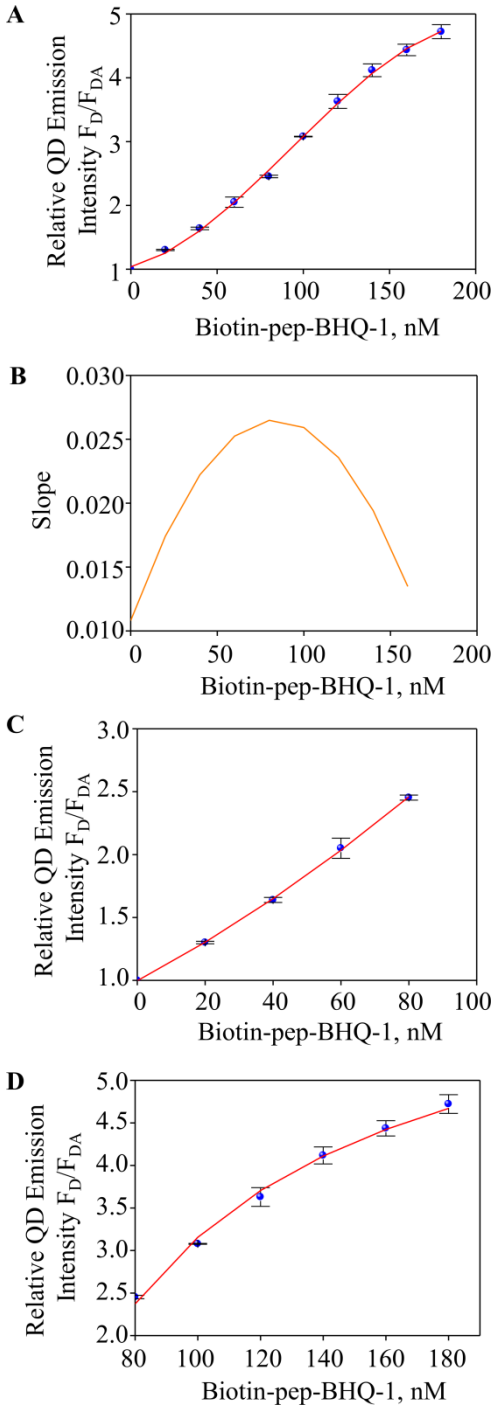

Figure 16. Stern-Volmer plots showing change in the PL intensity (F_D/F_{DA}) of QD525 (F_D) upon titration against biotin-pep-BHQ-1 (F_{DA}). (**A**) plot of 3 nM QD titrated against 0-180 nM biotin-pep-BHQ-1; the data points are connected using sigmoidal fit as guide to eyes. (**B**) plot of slope of each data point against the concentration of biotin-pep-BHQ-1 and (**C**) and **(D)** plots of 3 nM QD titrated against 0-80 nM and 80-120 biotin-pep-BHQ-1, respectively.

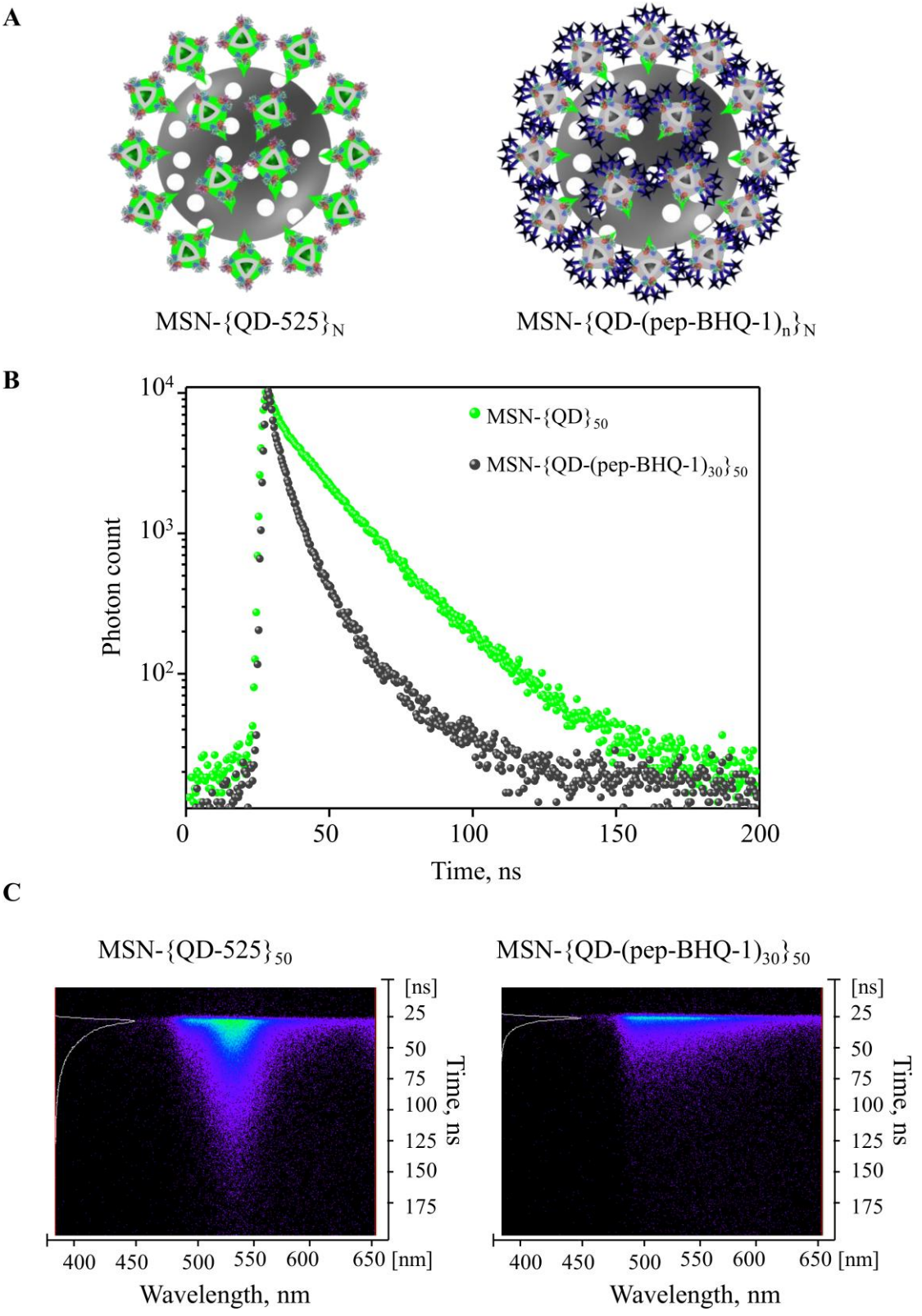

Figure 17. Nanobioassemblies and their PL properties. (A) Schematic representation

of MSN-$(QD525)_N$ and MSN-$[QD\text{-}(pep\text{-}BHQ\text{-}1)_n]_N$ nanobioassembly. (B) PL decay profiles of MSN-$(QD525)_N$ and MSN-$[QD\text{-}(pep\text{-}BHQ\text{-}1)_n]_N$ nanobioassembly. QDs are excited at 400 nm where the direct absorption of excitation light by BHQ-1 is minimum; as we employ PL lifetime of the donor in the estimation of FRET efficiency, any residual absorption of excitation light by BHQ-1 does not affect the measured FRET values. (C) Wavelength-resolved PL delay profiles of MSN-$(QD525)_N$ and MSN-$[QD\text{-}(pep\text{-}BHQ\text{-}1)_n]_N$ nanobioassembly.

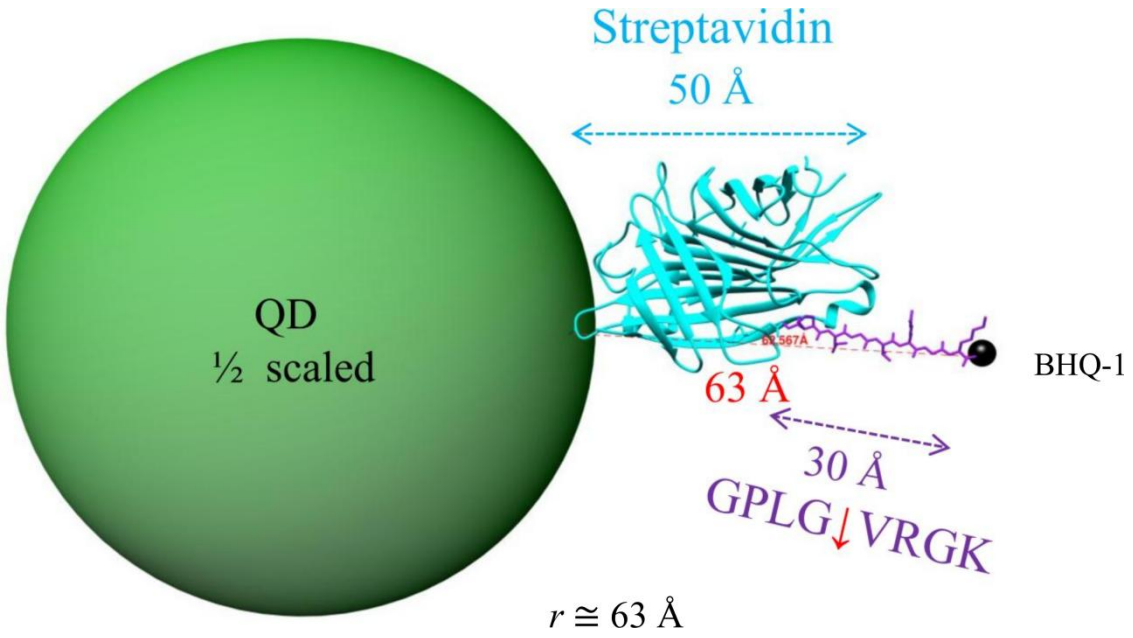

Figure 18. Models of single biotin labeled GPLGVRGK peptide conjugated to the streptavidin labeled QD in the extended position. The modeling was done using UCSF Chimera molecular modeling software.

Table 4. Individual decay components and average lifetimes of QD525 in MSN-$(QD525)_N$ and MSN-$[QD\text{-}(pep\text{-}BHQ\text{-}1)_n]_N$ conjugates.

Sample	τ_1 **(ns)**	τ_2 **(ns)**	τ_3 **(ns)**	A_1	A_2	A_3	τ_{av} **(ns)**
MSN-$\{QD\}_{50}$	2.334	17.349	56.502	0.298	0.682	0.259	13.90±0.52
MSN-$\{QD\text{-}(pep\text{-}BHQ\text{-}1)_{30}\}_{50}$	1.710	5.735	21.453	0.401	0.564	0.069	5.22± 0.51

QD decay profiles were fitted with a third order exponential function.

Chapter 4. Optical Sensing of Matrix Metalloproteinase-2 by using QD-pep-BHQ-1 nanoassembly

4.1 Introduction

The extra cellular matrix (ECM) of cancer cells in tumours and non cancerous stromal cells inside tumours potentiate cancer progression.[107] Matrix metalloproteinase are secreted as zymogen usually by stromal cells such as fibroblast.[108]

As shown in Figure 19 MMP-2 protein structure contain an amino-terminal signal sequence (Pre) that directs them to the endoplasmic reticulum, a propeptide (Pro) with a zinc-interacting thiol (SH) group that maintains them as inactive zymogens and a catalytic domain with a zinc-binding site (Zn), hemopexin domain which is connected to the catalytic domain by a hinge (H) that mediates interactions with tissue inhibitors of metalloproteinases, cell-surface molecules and proteolytic substrates. The first and the last of the four repeats in the hemopexin domain are linked by a disulphide bond (S–S). It also shows a series of three head-to-tail cysteine-rich repeats within its catalytic domain. These inserts resemble the collagen-binding type II repeats of fibronectin and are required to bind and cleave collagen and elastin.[109] MMP-2s are first produced as latent pro-MMPs with a pro-domain blocking the active site. The removal of the pro-domain is required to activate MMPs by revealing the zinc ion in the catalytic site. The cysteine-switch activation mechanism are widely used to activate MMPs, which is the removal of cysteine residues from the complex formed between cysteine residues in the pro-peptide domain and the essential zinc atom in the catalytic domain.[110,111] Active MMPs are then able to cleave substrates. The activity of MMPs is regulated by interaction with TIMPs, which inactivate the MMPs. But at the cell surface MMP-2 is

activated through multistep process which is mediated by MMP-14(Membrane type 1 or MT1-MMP) and tissue inhibitor of metalloproteinase 2 (TIMP-2).[112] TIMP-2 binds pro-MMP-2 at its carboxyl terminus and MT1-MMP at its amino terminus. Already activated MMP-2 is required to remove a residual portion of the pro domain of MMP-2.[113] Zymogen MMP-2 can also be activated without the presence of TIMP-2 but through another mechanism by MMP-15.[114] In this chapter discusses the sensing of activated MMP-2 in solution as wells its further detection at the ECM of H1299 cancer cells using QD-(pep-BHQ-1)$_n$ nanobioassembly.

4.2 Materials

a) Donor

Streptavidin modified CdSe/ZnS QD samples with emission intensity maximum ca 585 nm (QD585), Life Technologies (Tokyo, Japan). The streptavidin-QD585 solution was diluted to 3 nM in prepared TCNB buffer.

b) Acceptor

A short peptide containing PLGVR amino acid sequences were designed to be biotin-Glycine-Proline-Leucine-Glycine-Valine-Arginine-(Lysine-BHQ-1)-$CONH_2$ or biotin-GPLG↓VRG(Lys[BHQ-1])-$CONH_2$, and custom made with 99% purity was purchased from Custom Peptide & Antibody Service, Eurofins Genomics K.K. (Tokyo, Japan). The ample was further diluted with TCNB buffer solution.

c) MMP-2 samples and buffer

Activated MMP-2 was purchased from (Calbiochem, USA); pro-MMP-2 (human MMP-2, Recombinant, Anaspec, USA) and the TCNB buffer (50 mM Tris, 10 mM $CaCl_2$, 150 mM NaCl, and 0.01% Brij35; pH 7.5) was prepared using 50 mM Tris

(Wako), 10 mM $CaCl_2$ (Sigma), 150 mM NaCl (Sigma), and 0.01% Brij35 (Thermo Scientific); and the pH was monitored using a pH meter (Horiba, Japan).

d) Cancer Cell samples

H1299 cancer cells were purchased from. Dulbecco's modified eagle medium (DMEM) purchased from Thermo Fisher Scientific (Tokyo, Japan). Fetal bovine serum (FBS) was purchased from Trace Scientific Ltd. (Melbourne, Australia). Cell counting chamber slide Countess, Invitrogen, Tokyo, Japan. Trypan blue stain (0.4%), gibco, Life technology, (Tokyo, Japan).

4.3 Methods

a) Conjugation of donor and acceptor in buffer

3 nM streptavidin QD585 sample is incubated with 120 nM biotin-pep-BHQ-1 overnight in TCNB buffer solution.

b) Steady state photoluminescence spectroscopy

The steady state PL recovery from MMP-2 activity and control experiment measured by using fluorescence spectrophotometer F-4500 (Hitachi, Tokyo, Japan)

c) Cell culture experiment

H1299 cancer cells were cultured in DMEM, 10% FBS medium on a bio clean bunch (Astech, Tokyo, Japan). The QD-pep-BHQ-1 were incubated with the cell cultures for 1 hour and four hours respectively in a CO_2 incubator (Sanyo,Tokyo, Japan) at 37^{o}C.

d) Multiphoton confocal microscopy

The cell imaging were performed with a high speed multiphoton confocal laser microscopy ($A1MP^{+}$ /$A1RMP^{+}$, Nikon, Tokyo, Japan). The cells were imaged at the multiphon mode using an 800 nm wavelength laser pulses from a Ti:saphire fempto second laser.

4.3 Results and Discussion

a) Control experiment to check the stability of nanobioassembly

As a control experiment the stability of the QD-pep-BHQ-1 nanoassembly were incubated with pro-MMP-2 at 37°C temperature for prolonged time period. Another control was also checked without the presence of MMP-2 sample. In this case QD-pep-BHQ-1 nanobioassembly were incubated at 37°C for prolonged time. The measurement was performed between 10 and 4 minute time gap respectively and excited under 400 nm for more than an hour in each case. It was observed that the nanobioassembly remained unchanged and continued its PL quenched state without any degradation during the entire measurement as shown in Figure 20 and Figure 21.

b) Detection of MMP-2

A limit of detection of 1 ng/mL (15 pM) concentration of MMP-2 was selected for detection experiment from the knowledge previous MMP-2 sensing experiment with energy transfer technology. Yao *et al*. described the detection of MMP-2 at a detection limit of 2 ng/mL with a QD/BRET nanosensor with a 10 % decrease in BRET ratio,[115] Shi *et al*. detected at a detection limit of 0.5 μg/mL with the developed QD based FRET sensor.[116] Zhao *et al*. detected MMP-2 at a detection limit of 19 ng/mL with a developed magnetic sensor.[117] 1 ng/mL of activated sample of MMP-2 incubated with the QD585-$(pep\text{-}BHQ\text{-}1)_{40}$ nanobioassembly in TCNB buffer at 37°C for two hours. Figure 22A describes the process of MMP-2 detection experiment with QD-$(pep\text{-}BHQ\text{-}1)_n$ nanobioassembly. The FRET signal transduction between the QD donor and BHQ-1 acceptor has broken by the catalytic activity of MMP-2 over the PLGVR amino acid sequence containing donor-acceptor bridging short peptide in the QD-$(pep\text{-}BHQ\text{-}1)_n$ nanobioassembly resulting a clear 20% PL recovery of QD585 from

PL quenched state, which is described in Figure 22B.

c) Detection of MMP-2 at the ECM of cancer cells

Figure 23 describes the detection of MMP-2 at the extra cellular matrix of H1299 cancer cells. QD 585-(pep-BHQ-1)$_{40}$ were incubated with H1299 cancer cell at a cell count of 2.5 $\times 10^4$ cells/ml. Figure 23A and 23B shows the MMP-2 detection images after 1 hour incubation. Figure 23C, 23D and 23E shows MMP-2 detection images after 4 hours of incubation. It is clear that upon increasing the incubation time, the number of cells increases as well as more MMP-2s get activated at the cell surfaces. As reported MMP-2 produced as zymogen (pro-state) inside the cell and were either discharged into the cytoplasm or docked to the cell surface integrin receptors. Usually in cancer cells MMPs were localized at the integrin receptors of the cell membrane in the active form. In this case the QD-(pep-BHQ-1)$_n$ nanoassembly is just tethered to the ECM of H1299 cancer cell cultures and there was no aim to target or adhere to any specific site of the cell membrane.

4.4 Conclusion

The QD-(pep-BHQ-1)$_n$ nanobioassembly sensitively detected MMP-2 by breaking the FRET signal transduction between QD donor and BHQ-1 acceptor at a detection limit of 1 ng/mL. The higher sensitivity of the nanobioassembly compared to the previously reported QD based nanosensors can be assigned to the non-emissive background of the BHQ-1 acceptor with a large value of molar extinction coefficient. The QD-(pep-BHQ-1)$_n$ conjugate also sensitively detected and imaged the MMP-2 presence at the extra cellular matrix of H1299 cancer cells.

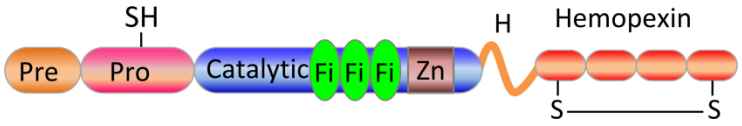

Figure 19. The protein structure of matrix metalloproteinase -2 (MMP-2).

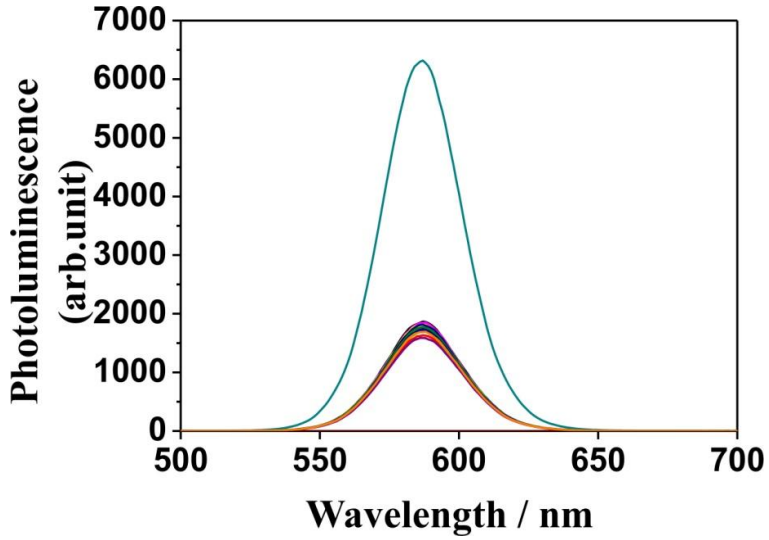

Figure 20. Steady state PL time evolution spectra of QD585 upon Pro-MMP-2 reaction on QD-(pep-BHQ-1)$_{40}$ conjugates recorded at 37°C temperatures. The measurement was repeated at successive interval of 10 minute time gap. The sample was excited at 400 nm.

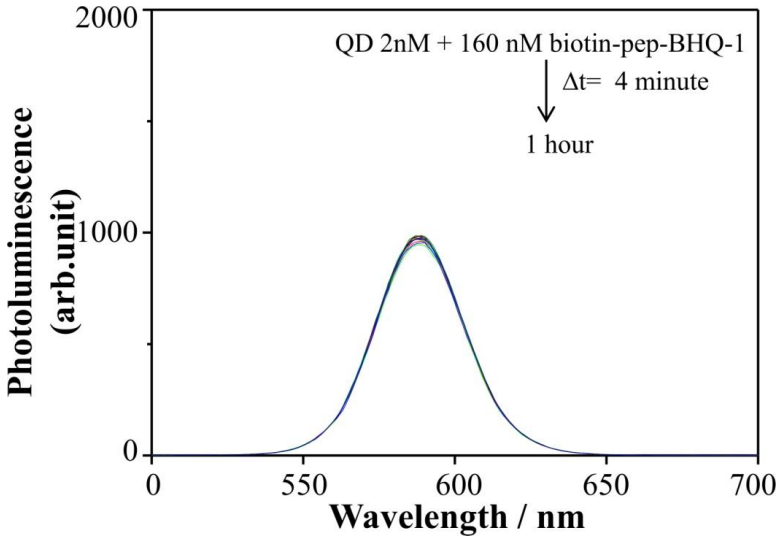

Figure 21. Steady state PL time evolution spectra of QD-(pep- BHQ-1)$_{80}$ conjugates recorded at 37°C. The measurements were repeated at successive interval of 4 minute time gap.

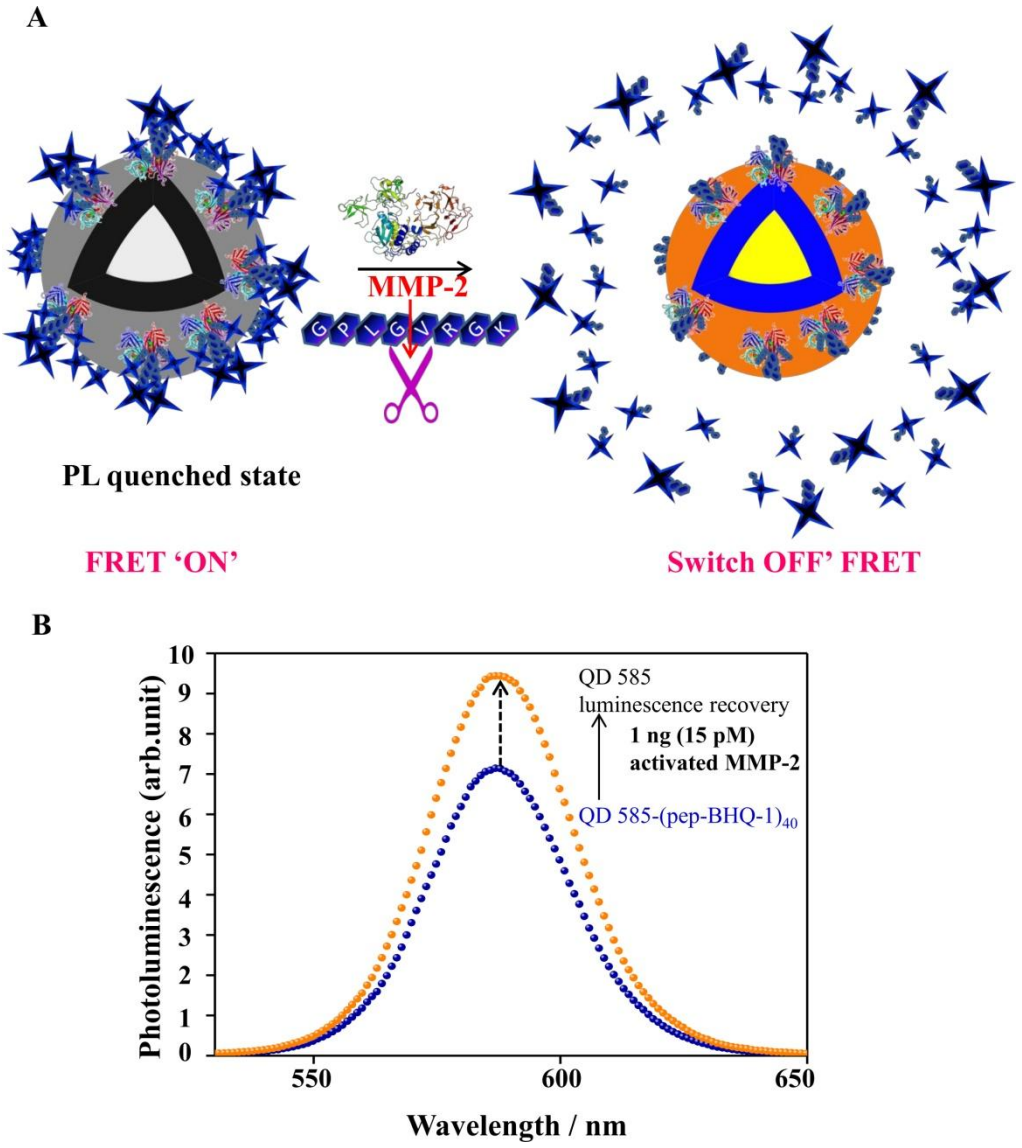

Figure 22. A. Hypothesis about FRET mediated PL quenching of QDs followed by sensitive detection of MMP-2 using QD-(pep-BHQ-1)$_n$ nanobioassembly. B. Detection of MMP-2 with QD-(pep-BHQ-1)$_n$ nanobioassembly. The QD-(pep-BHQ-1)$_{40}$ nanobioassembly were incubated with activated MMP-2 (1 ng/mL) for two hours at 37°C before FRET measurement. From bottom to top the black line shows the PL quenched state and the red line shows the recovered PL spectra of QD585 after 2 hours of incubation with 1 ng/mL of activated MMP-2.

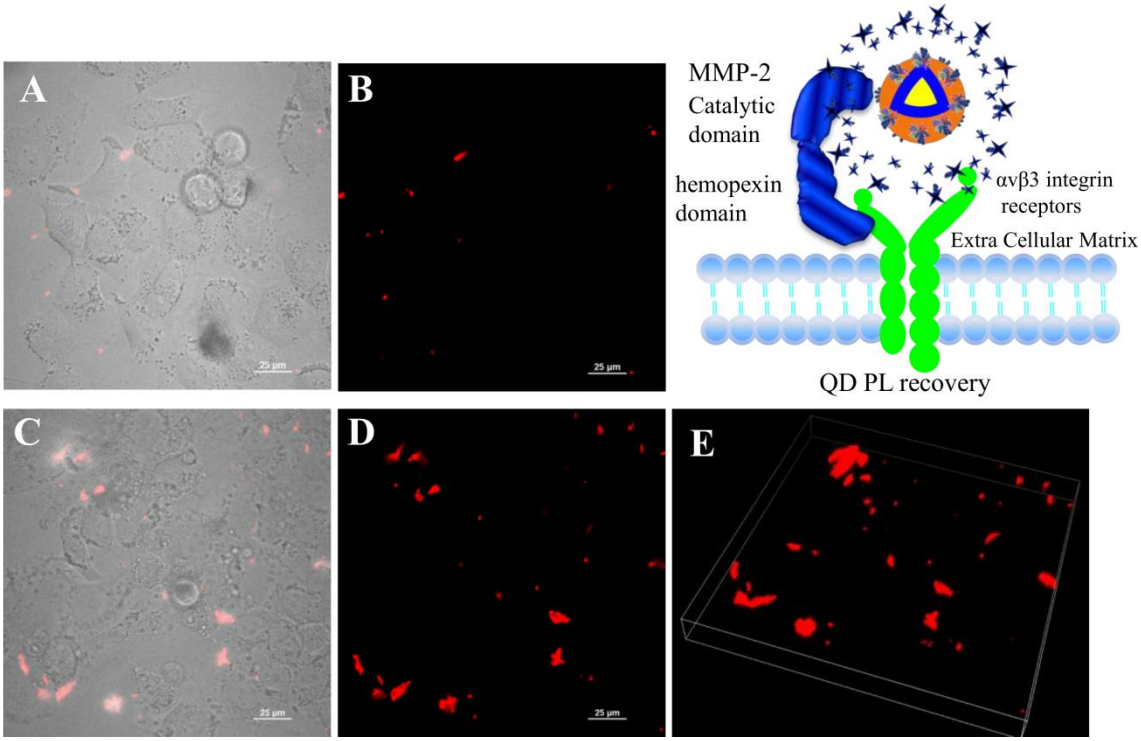

Figure 23. Multi photon confocal microscopy images of QD585-(pep-BHQ-1)$_n$ conjugates in H1299 cell culture. A and B incubated for 1 hour. C.D and E incubated for 4 hours. Schematic shows the luminescence recovery of QD585 from QD585-(pep-BHQ-1)$_{40}$ quenched state after interaction with the MMP-2 localized at the αvβ3 integrin receptors.

Chapter 5. Concluding Remarks and Future Perspectives

Successfully conjugated the QD and biotin-pep-BHQ-1 molecule and made the QD-(pep-BHQ-1)$_n$ nanobioassembly. The QD PL is efficiently quenched by biotin-pep-BHQ-1 molecules. Calculated the apparent conjugation ratios of QD-pep-BHQ-1 nanoassembly and the corresponding FRET efficiencies were measured using both steady state and time-resolved spectroscopy. After that successfully conjugated the QD-pep-BHQ-1 nanobioassembly on mesoporous silica nanoparticle and made the MSN-[QD-(pep-BHQ-1)$_n$]$_N$ nanobioassembly. The QD photoluminescence is efficiently quenched by biotin-pep-BHQ-1 molecule on the surface of MSN. Calculated the apparent MSN-{QD-(pep-BHQ-1)$_{30}$}$_{50}$ nanobioassembly conjugation ratios and the corresponding FRET efficiencies were measured using time resolved spectroscopy. Finally the MMP-2 were sensitively detected at a limit of detection of 1 ng/mL with a clear luminescence recovery of QDs compared to the previously reported MMP-2 detection experiments. Successively successfully sensed and imaged the MMP-2 activity at the extra cellular matrix (ECM) of H1299 cancer cells with a confocal microscope to visualize the extra cellular matrix dynamic niche of cancer cells.

In Chapter 2 and 3 the MMP-2 target peptide is the bridging entity between QD donor and BHQ-1 acceptors. The conformation dynamics as well as the charge hoping properties of the short peptide were not taken into consideration. Ultrafast transient absorption spectroscopic measurement is needed to accurately understand energy transfer pathways and possibility of photo induced electron transfer in QD-pep-BHQ-1 nanobioassembly. Sophiticated technologies are required to unravel atom by atom dipole-dipole orientation and interaction dynamics to better understand

structure-function correlation of these nanobioassembly in order to do more advanced biosensing applications..

MMP-2 mediate the angiogenesis in tumours. The synthesized and characterized MSN-[QD-(pep-BHQ-1)$_n$]$_N$ conjugates with a n×N large number of localized target peptide in a nano space volume will be used for future targeted detection of MMP-2 at the αvβ3 integrin receptors of the cancer cell membrane to understand the upregulation in the extra cellular matrix dynamic niche of cancer cells. A hypothesis of the experiment is described in Figure 24.

Stem cells are localized in the stem-cell niche in the undifferentiated quiescent states. MMPs mediate the transfer of stem cells from the quiescent niche to the proliferative niche. The extra cellular matrix niche modulates the self-renewal, proliferation, and differentiation of stem cells, thus enabling continuous production of all type of mature cells. Hence sensing MMPs at the ECM of stem cells will aslo help to modulate stem cell differentiation for future regenerative medicine development and research.

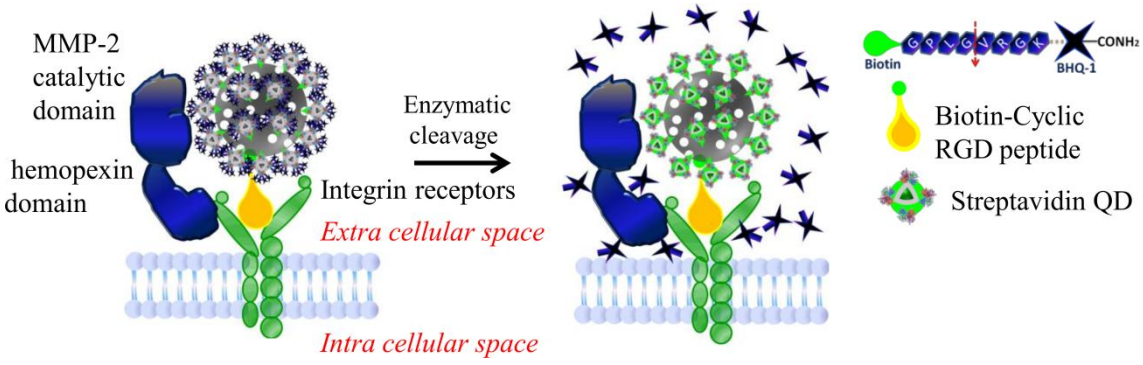

Figure 24. Future perspective. Hypothesis of MMP-2 detection at the αvβ3 integrin receptors, at the extra cellular matrix of cancer cells using MSN-[QD-(pep-BHQ-1)$_n$]$_N$ nanobioassembly.

Acknowledgements

I would like to express my sincere gratitude to Professor Yoshinobu Baba (Nagoya University) for his kind Guidance, constructive suggestion and continuous encouragement.

I would like to acknowledge Professor Noritada Kaji, Associate Professor Hiroshi Yukawa , Assistant Professor Takao Yasui and Assistant Professor Onoshima Daisuke.

I am also thankful to Prof. Vasudevan Biju for the valuable guidance and discussion at AIST, Takamatsu.

I would like to express my gratitude to Prof. Hiroshi Murakami, Prof. Hiromu Kashida, for valuable discussions.

I thank Assistant Professor Ashwin Selvarajan, Nagoya University for the fruitful discussions.

I am thankful to all members of Baba Lab.

This research is supported by the Japan Agency for Medical Research and Development (AMED) through its “Research Center Network for Realization of Regenerative Medicine”. MEXT for a JSPS Grant-in-Aid for scientific research on innovative areas “Photosynergetics” (Kaken-hi Grant # 15H01099) and partially supported by JSPS KAKENHI Grant Numbers JP26790006.

Not last but the least I am extremely thankful to my family members, relatives and friends for their great support and constant encouragement.

References

(1) Sternlicht, M. D.; Werb, Z. How Matrix Metalloproteinases Regulate Cell Behavior. *Annual Review of Cell and Developmental Biology* **2001**, *17* (1), 463–516.

(2) Coussens, L. M.; Werb, Z. Matrix Metalloproteinases and the Development of Cancer. *Chemistry & Biology* **1996**, *3* (11), 895–904.

(3) Egeblad, M.; Werb, Z. New Functions for the Matrix Metalloproteinases in Cancer Progression. *Nature Reviews Cancer* **2002**, *2* (3), 161–174.

(4) Mott, J. D.; Werb, Z. Regulation of Matrix Biology by Matrix Metalloproteinases. *Current Opinion in Cell Biology* **2004**, *16* (5), 558–564.

(5) Werb, Z. ECM and Cell Surface Proteolysis: Minireview Regulating Cellular Ecology. *Cell* **1997**, *91*, 439–442.

(6) Sternlicht, M. D.; Bergers, G. Matrix Metalloproteinases as Emerging Targets in Anticancer Therapy: Status and Prospects. *Emerging Therapeutic Targets* **2000**, *4* (5), 609–633.

(7) Sherwood, L. M.; Parris, E. E.; Folkman, J. Tumor Angiogenesis: Therapeutic Implications. *New England Journal of Medicine* **1971**, *285* (21), 1182–1186.

(8) Kim, K. J.; Li, B.; Winer, J.; Armanini, M.; Gillett, N.; Phillips, H. S.; Ferrara, N. Inhibition of Vascular Endothelial Growth Factor-Induced Angiogenesis Suppresses Tumour Growth in Vivo. *Nature* **1993**, *362* (6423), 841–844.

(9) Xu, J.; Rodriguez, D.; Petitclerc, E.; Kim, J. J.; Hangai, M.; Moon Yuen, S.; Davis, G. E.; Brooks, P. C. Proteolytic Exposure of a Cryptic Site within Collagen Type IV Is Required for Angiogenesis and Tumor Growth in Vivo. *The*

Journal of Cell Biology **2001**, *911* (5), 21–9525.

(10) Brooks, P. C.; Strömblad, S.; Sanders, L. C.; von Schalscha, T. L.; Aimes, R. T.; Stetler-Stevenson, W. G.; Quigley, J. P.; Cheresh, D. A. Localization of Matrix Metalloproteinase MMP-2 to the Surface of Invasive Cells by Interaction with Integrin αvβ3. *Cell* **1996**, *85* (5), 683–693.

(11) Seltzer, J. L.; Akers, K. T.; Weingarten, H.; Grant, G. A.; McCourt, D. W.; Eisen, A. Z. Cleavage Specificity of Human Skin Type IV Collagenase (Gelatinase). Identification of Cleavage Sites in Type I Gelatin, with Confirmation Using Synthetic Peptides. *The Journal of biological chemistry* **1990**, *265* (33), 20409–20413.

(12) Hynes, R. O. Integrins: Versatility, Modulation, and Signaling in Cell Adhesion. *Cell* **1992**, *69* (1), 11–25.

(13) Miranti, C. K.; Brugge, J. S. Sensing the Environment: A Historical Perspective on Integrin Signal Transduction. *Nature Cell Biology* **2002**, *4* (4), E83–E90.

(14) Lu, P.; Weaver, V. M.; Werb, Z. The Extracellular Matrix: A Dynamic Niche in Cancer Progression. *The Journal of Cell Biology* **2012**, *196* (4), 395–406.

(15) Kamat, P. V. Quantum Dot Solar Cells. *The Next Big Thing* in Photovoltaics. *The Journal of Physical Chemistry Letters* **2013**, *4* (6), 908–918.

(16) Klimov, V. I.; Mikhailovsky, A. A.; Xu, S.; Malko, A.; Hollingsworth, J. A.; Leatherdale, C. A.; Eisler, H.; Bawendi, M. G.; Mehus, D.; Evans, D.; et al. Optical Gain and Stimulated Emission in Nanocrystal Quantum Dots. *Science (New York, N.Y.)* **2000**, *290* (5490), 314–317.

(17) Klimov, V. I.; Ivanov, S. A.; Nanda, J.; Achermann, M.; Bezel, I.; McGuire, J. A.; Piryatinski, A. Single-Exciton Optical Gain in Semiconductor Nanocrystals.

Nature **2007**, *447* (7143), 441–446.

(18) Imamoğlu, A.; Michler, P.; Mason, M. D.; Carson, P. J.; Strouse, G. F.; Buratto, S. K. Quantum Correlation among Photons from a Single Quantum Dot at Room Temperature. *Nature* **2000**, *406* (6799), 968–970.

(19) Aichele, T.; Zwiller, V.; Benson, O.; Akimov, I.; Henneberger, F. Single CdSe Quantum Dots for High-Bandwidth Single-Photon Generation. *Journal of the Optical Society of America B* **2003**, *20* (10), 2189.

(20) Colvin, V. L.; Schlamp, M. C.; Alivisatos, A. P. Light-Emitting Diodes Made from Cadmium Selenide Nanocrystals and a Semiconducting Polymer. *Nature* **1994**, *370* (6488), 354–357.

(21) Bourzac, K. Quantum Dots Go on Display. *Nature* **2013**, *493* (7432), 283.

(22) Bakalova, R.; Ohba, H.; Zhelev, Z.; Ishikawa, M.; Baba, Y. Quantum Dots as Photosensitizers? *Nature Biotechnology* **2004**, *22* (11), 1360–1361.

(23) Bakalova, R.; Ohba, H.; Zhelev, Z.; Nagase, T.; Jose, R.; Ishikawa, M.; Baba, Y. Quantum Dot Anti-CD Conjugates: Are They Potential Photosensitizers or Potentiators of Classical Photosensitizing Agents in Photodynamic Therapy of Cancer? *Nano Letters* **2004**, *4* (9), 1567–1573.

(24) Bakalova, R.; Zhelev, Z.; Ohba, H.; Baba, Y. Quantum Dot-Based Western Blot Technology for Ultrasensitive Detection of Tracer Proteins. *Journal of the American Chemical Society* **2005**, *127* (26), 9328–9329.

(25) Sugawa, M.; Nishikawa, S.; Iwane, A. H.; Biju, V.; Yanagida, T. Single-Molecule FRET Imaging for Enzymatic Reactions at High Ligand Concentrations. *Small* **2010**, *6* (3), 346–350.

(26) Hanne, J.; Falk, H. J.; Görlitz, F.; Hoyer, P.; Engelhardt, J.; Sahl, S. J.; Hell, S. W.

STED Nanoscopy with Fluorescent Quantum Dots. *Nature Communications* **2015**, *6*, 7127.

(27) Somers, R. C.; Bawendi, M. G.; Nocera, D. G. CdSe Nanocrystal Based Chem-/bio- Sensors. *Chemical Society reviews* **2007**, *36* (4), 579–591.

(28) Jares-Erijman, E. A.; Jovin, T. M. FRET Imaging. *Nature Biotechnology*. Nature Publishing Group November 2003, pp 1387–1395.

(29) Miyawaki, A. Visualization of the Spatial and Temporal Dynamics of Intracellular Signaling. *Developmental cell* **2003**, *4* (3), 295–305.

(30) Sapsford, K. E.; Berti, L.; Medintz, I. L. Materials for Fluorescence Resonance Energy Transfer Analysis: Beyond Traditional Donor–Acceptor Combinations. *Angewandte Chemie International Edition* **2006**, *45* (28), 4562–4589.

(31) Clapp, A. R.; Medintz, I. L.; Mattoussi, H. Förster Resonance Energy Transfer Investigations Using Quantum-Dot Fluorophores. *ChemPhysChem*. WILEY-VCH Verlag January 16, 2006, pp 47–57.

(32) Michalet, X.; Pinaud, F.; Lacoste, T. D.; Dahan, M.; Bruchez, M. P.; Alivisatos, A. P.; Weiss, S. Properties of Fluorescent Semiconductor Nanocrystals and Their Application to Biological Labeling. *Single Molecules* **2001**, *2* (4), 261–276.

(33) Medintz, I. L.; Uyeda, H. T.; Goldman, E. R.; Mattoussi, H. Quantum Dot Bioconjugates for Imaging, Labelling and Sensing. *Nature Materials* **2005**, *4* (6), 435–446.

(34) Alivisatos, A. P.; Gu, W.; Larabell, C. Quantum Dots as Cellular Probes. *Annual Review of Biomedical Engineering* **2005**, *7* (1), 55–76.

(35) Alivisatos, P. The Use of Nanocrystals in Biological Detection. *Nature Biotechnology* **2004**, *22* (1), 47–52.

(36) Klostranec, J. M.; Chan, W. C. W. Quantum Dots in Biological and Biomedical Research: Recent Progress and Present Challenges. *Advanced Materials* **2006**, *18* (15), 1953–1964.

(37) Chan, W. C.; Nie, S. Quantum Dot Bioconjugates for Ultrasensitive Nonisotopic Detection. *Science (New York, N.Y.)* **1998**, *281* (5385), 2016–2018.

(38) Nirmal, M.; Dabbousi, B. O.; Bawendi, M. G.; Macklin, J. J.; Trautman, J. K.; Harris, T. D.; Brus, L. E. Fluorescence Intermittency in Single Cadmium Selenide Nanocrystals. *Nature* **1996**, *383* (6603), 802–804.

(39) Kuno, M.; Fromm, D. P.; Hamann, H. F.; Gallagher, A.; Nesbitt, D. J. "On"/"off" Fluorescence Intermittency of Single Semiconductor Quantum Dots. *The Journal of Chemical Physics* **2001**, *115* (2), 1028–1040.

(40) Kuno, M.; Fromm, D. P.; Johnson, S. T.; Gallagher, A.; Nesbitt, D. J. Modeling Distributed Kinetics in Isolated Semiconductor Quantum Dots. *Physical Review B* **2003**, *67* (12), 125304.

(41) Walkey, C. D.; Chan, W. C. W. Understanding and Controlling the Interaction of Nanomaterials with Proteins in a Physiological Environment. *Chemical Society reviews* **2012**, *41* (7), 2780–2799.

(42) Mattoussi, H.; Mauro, J. M.; Goldman, E. R.; Anderson, G. P.; Sundar, V. C.; Mikulec, F. V.; Bawendi, M. G. Self-Assembly of CdSe−ZnS Quantum Dot Bioconjugates Using an Engineered Recombinant Protein. *Journal of the American Chemical Society* **2000**, *122* (49), 12142–12150.

(43) Dale M. Willard; Carillo, L. L.; Jung, J.; Orden, A. Van. CdSe − ZnS Quantum Dots as Resonance Energy Transfer Donors in a Model Protein − Protein Binding Assay. *Nano Letters* **2001**, No. 2.

(44) Willard, D. M.; Carillo, L. L.; Jung, J.; Van Orden, A. CdSe-ZnS Quantum Dots as Resonance Energy Transfer Donors in a Model Protein-Protein Binding Assay. *Nano Letters* **2001**, *1* (9), 469–474.

(45) Clapp, A. R.; Medintz, I. L.; Mauro, J. M.; Fisher, B. R.; Bawendi, M. G.; Mattoussi, H. Fluorescence Resonance Energy Transfer Between Quantum Dot Donors and Dye-Labeled Protein Acceptors. *Journal of the American Chemical Society* **2004**, *126* (1), 301–310.

(46) Tran, P. T.; Anderson, G. P.; Mauro, J. M.; Mattoussi, H. Use of Luminescent CdSe-ZnS Nanocrystal Bioconjugates in Quantum Dot-Based Nanosensors. *physica status solidi (b)* **2002**, *229* (1), 427–432.

(47) Hohng, S.; Ha, T. Single-Molecule Quantum-Dot Fluorescence Resonance Energy Transfer. *ChemPhysChem* **2005**, *6* (5), 956–960.

(48) Zhou, D.; Piper, J. D.; Abell, C.; Klenerman, D.; Kang, D.-J.; Ying, L. Fluorescence Resonance Energy Transfer between a Quantum Dot Donor and a Dye Acceptor Attached to DNA. *Chemical Communications* **2005**, *0* (38), 4807.

(49) Clapp, A. R.; Medintz, I. L.; Fisher, B. R.; Anderson, G. P.; Mattoussi, H. Can Luminescent Quantum Dots Be Efficient Energy Acceptors with Organic Dye Donors? *Journal of the American Chemical Society* **2005**, *127* (4), 1242–1250.

(50) Murray, C. B.; Norris, D. J.; Bawendi, M. G. Synthesis and Characterization of Nearly Monodisperse CdE (E = Sulfur, Selenium, Tellurium) Semiconductor Nanocrystallites. *Journal of the American Chemical Society* **1993**, *115* (19), 8706–8715.

(51) Qu, L.; Peng, X. Control of Photoluminescence Properties of CdSe Nanocrystals in Growth. *Journal of the American Chemical Society* **2002**, *124* (9), 2049–2055.

(52) Brus, L. E. A Simple Model for the Ionization Potential, Electron Affinity, and Aqueous Redox Potentials of Small Semiconductor Crystallites. *The Journal of Chemical Physics* **1983**, *79* (11), 5566–5571.

(53) Klimov, V. I. Spectral and Dynamical Properties of Multiexcitons in Semiconductor Nanocrystals. *Annual Review of Physical Chemistry* **2007**, *58* (1), 635–673.

(54) Efros, A. L.; and Efros, A. L. Interband Absorption of Light in a Semiconductor Sphere. *Soviet Physics Semiconductors-Ussr* **1982**, *16* (7), 772–775.

(55) Efros, A. L.; Rosen, M. The Electronic Structure of Semiconductor Nanocrystals. *Annual review of material science* **2000**, *30*, 475–521.

(56) Brus, L. E. Electron–electron and Electron-hole Interactions in Small Semiconductor Crystallites: The Size Dependence of the Lowest Excited Electronic State. *The Journal of Chemical Physics* **1984**, *80* (9), 4403–4409.

(57) Jones, M.; Nedeljkovic, J.; Ellingson, R. J.; Nozik, A. J.; Rumbles, G. Photoenhancement of Luminescence in Colloidal CdSe Quantum Dot Solutions. *The Journal of Physical Chemistry B* **2003**, *107* (41), 11346–11352.

(58) Efros, A. L.; Kharchenko, V. A.; Rosen, M. Breaking the Phonon Bottleneck in Nanometer Quantum Dots: Role of Auger-like Processes. *Solid State Communications* **1995**, *93* (4), 281–284.

(59) Nirmal, M.; Brus, L. Luminescence Photophysics in Semiconductor Nanocrystals. *Accounts of Chemical Research*. 1999, pp 407–414.

(60) Underwood, D. F.; Kippeny, T.; Rosenthal, S. J. Ultrafast Carrier Dynamics in CdSe Nanocrystals Determined by Femtosecond Fluorescence Upconversion Spectroscopy. *The Journal of Physical Chemistry B* **2001**, *105* (2), 436–443.

(61) Klimov, V. I.; McBranch, D. W.; Leatherdale, C. A.; Bawendi, M. G. Electron and Hole Relaxation Pathways in Semiconductor Quantum Dots. *Physical Review B* **1999**, *60* (19), 13740–13749.

(62) Sewall, S.; Cooney, R.; Anderson, K.; Dias, E.; Kambhampati, P. State-to-State Exciton Dynamics in Semiconductor Quantum Dots. *Physical Review B* **2006**, *74* (23), 1–8.

(63) Cooney, R. R.; Sewall, S. L.; Anderson, K. E. H.; Dias, E. A.; Kambhampati, P. Breaking the Phonon Bottleneck for Holes in Semiconductor Quantum Dots. *Physical Review Letters* **2007**, *98* (17).

(64) Ekimov, A. I.; Kudryavtsev, I. A.; Efros, A. L.; Yazeva, T. V.; Hache, F.; Schanne-Klein, M. C.; Rodina, A. V.; Ricard, D.; Flytzanis, C. Absorption and Intensity-Dependent Photoluminescence Measurements on CdSe Quantum Dots: Assignment of the First Electronic Transitions. *Journal of the Optical Society of America B* **1993**, *10* (1), 100.

(65) Efros, A. L.; Rodina, A. V. Band-Edge Absorption and Luminescence of Nonspherical Nanometer-Size Crystals. *Physical Review B* **1993**, *47* (15), 10005–10007.

(66) Efros, A. L. Luminescence Polarization of CdSe Microcrystals. *Physical Review B* **1992**, *46* (12), 7448–7458.

(67) Norris, D. J.; Bawendi, M. G. Measurement and Assignment of the Size-Dependent Optical Spectrum in CdSe Quantum Dots. *Physical Review B* **1996**, *53* (24), 16338–16346.

(68) Nirmal, M.; Norris, D. J.; Kuno, M.; Bawendi, M. G.; Efros, A. L.; Rosen, M. Observation of The “dark Exciton” in CdSe Quantum Dots. *Physical Review*

Letters **1995**, *75* (20), 3728–3731.

(69) Efros, A. L.; Rosen, M.; Kuno, M.; Nirmal, M.; Norris, D. J.; Bawendi, M. Band-Edge Exciton in Quantum Dots of Semiconductors with a Degenerate Valence Band: Dark and Bright Exciton States. *Physical Review B* **1996**, *54* (7), 4843–4856.

(70) Hines, M. A.; Guyot-Sionnest, P. Synthesis and Characterization of Strongly Luminescing ZnS-Capped CdSe Nanocrystals. *The Journal of Physical Chemistry* **1996**, *100* (2), 468–471.

(71) Shibu, E. S.; Hamada, M.; Nakanishi, S.; Wakida, S.-I.; Biju, V. Photoluminescence of CdSe and CdSe/ZnS Quantum Dots: Modifications for Making the Invisible Visible at Ensemble and Single-Molecule Levels. *Coordination Chemistry Reviews* **2014**, *263–264* (264), 2–12.

(72) Jing, L.; Kershaw, S. V.; Li, Y.; Huang, X.; Li, Y.; Rogach, A. L.; Gao, M. Aqueous Based Semiconductor Nanocrystals. *Chemical Reviews* **2016**, *116* (18), 10623–10730.

(73) Harris, R. D.; Bettis Homan, S.; Kodaimati, M.; He, C.; Nepomnyashchii, A. B.; Swenson, N. K.; Lian, S.; Calzada, R.; Weiss, E. A. Electronic Processes within Quantum Dot-Molecule Complexes. *Chemical Reviews*. American Chemical Society November 9, 2016, pp 12865–12919.

(74) Vilan, A.; Cahen, D. Chemical Modification of Semiconductor Surfaces for Molecular Electronics. *Chemical Reviews* **2017**, *117* (5), 4624–4666.

(75) Tan, L.; Li, P.; Sun, B.; Chaker, M.; Ma, D. Stabilities Related to Near-Infrared Quantum Dot-Based Solar Cells: The Role of Surface Engineering. *ACS Energy Letters* **2017**, *2* (7), 1573–1585.

(76) Hines, D. A.; Kamat, P. V. Recent Advances in Quantum Dot Surface Chemistry. *ACS Applied Materials & Interfaces* **2014**, *6* (5), 3041–3057.

(77) Palato, S.; Seiler, H.; McGovern, L.; Mack, T. G.; Jethi, L.; Kambhampati, P. Electron Dynamics at the Surface of Semiconductor Nanocrystals. *The Journal of Physical Chemistry C* **2017**, *121* (47), 26519–26527.

(78) Margraf, J. T.; Ruland, A.; Sgobba, V.; Guldi, D. M.; Clark, T. Theoretical and Experimental Insights into the Surface Chemistry of Semiconductor Quantum Dots. *Langmuir* **2013**, *29* (49), 15450–15456.

(79) Perrin, J. B. Fluorescence et Lois Générales Relatives Aux Vitesses de Réaction. *Comptes rendus hebdomadaires des séances de l'Académie des Sci* **1924**, *178*, 1401–1406.

(80) Perrin, J. B. Fluorescence et Induction Moleculaire Par Resonance. *Comptes rendus hebdomadaires des séances de l'Académie des Sci* **1927**, *184*, 1097–1100.

(81) Perrin, F. Théorie Quantique Des Transferts D'activation Entre Molécules de Même Espèce. Cas Des Solutions Fluorescentes. *Annales de Physique* **1932**, *10* (17), 283–314.

(82) Forster, T. Energiewanderung Und Fluoreszenz. *Die Naturwissenschaften* **1946**, *33* (6), 166–175.

(83) Förster, T. Zwischenmolekulare Energiewanderung Und Fluoreszenz. *Annalen der Physik* **1948**, *437* (1–2), 55–75.

(84) Főrster, T. 10th Spiers Memorial Lecture. Transfer Mechanisms of Electronic Excitation. *Discussions of the Faraday Society* **1959**, *27* (0), 7–17.

(85) Förster, T. Experimentelle Und Theoretische Untersuchung Des Zwischenmolekularen Übergangs von Elektronenanregungsenergie. *Zeitschrift*

für Naturforschung **1949**, *4a*, 321–327.

(86) Förster, T. (1965). *Delocalized Excitation and Excitation Transfer. In: Modern Quantum Chemistry, Section III B, Action of Light and Organic Crystals*; O. Sinanoglu, Ed.; Academic Press: New York. pp 93-137.

(87) Stryer, L.; Haugland, R. P. Energy Transfer: A Spectroscopic Ruler. *Proceedings of the National Academy of Sciences of the United States of America* **1967**, *58* (2), 719–726.

(88) Stryer, L. Fluorescence Energy Transfer as a Spectroscopic Ruler. *Annual review of biochemistry* **1978**, *47*, 819–846.

(89) Lakowicz, J. R. *Principles of Fluorescence Spectroscopy*; Lakowicz, J. R., Ed.; Springer US: Boston, MA, 2006.

(90) *FRET - Förster Resonance Energy Transfer: From Theory to Application*; Medintz, I., Hildebrandt, N., Eds.; Wiley-VCH Verlag GmbH & Co. KGaA: Weinheim, Germany, 2013.

(91) Dale, R. E.; Eisinger, J. Intramolecular Distances Determined by Energy Transfer. Dependence on Orientational Freedom of Donor and Acceptor. *Biopolymers* **1974**, *13* (8), 1573–1605.

(92) Bawendi, M. G.; Wilson, W. L.; Rothberg, L.; Carroll, P. J.; Jedju, T. M.; Steigerwald, M. L.; Brus, L. E. Electronic Structure and Photoexcited-Carrier Dynamics in Nanometer-Size CdSe Clusters. *Physical Review Letters* **1990**, *65* (13), 1623–1626.

(93) Norris, D. J.; Nirmal, M.; Murray, C. B.; Sacra, A.; Bawendi, M. G. Size Dependent Optical Spectroscopy of II-VI Semiconductor Nanocrystallites (Quantum Dots). *Zeitschrift für Physik D Atoms, Molecules and Clusters* **1993**,

26 (1), 355–357.

(94) Mittleman, D. M.; Schoenlein, R. W.; Shiang, J. J.; Colvin, V. L.; Alivisatos, A. P.; Shank, C. V. Quantum Size Dependence of Femtosecond Electronic Dephasing and Vibrational Dynamics in CdSe Nanocrystals. *Physical Review B* **1994**, *49* (20), 14435–14447.

(95) Wang, H.; De Mello Donegá, C.; Meijerink, A.; Glasbeek, M. Ultrafast Exciton Dynamics in CdSe Quantum Dots Studied from Bleaching Recovery and Fluorescence Transients. *Journal of Physical Chemistry B* **2006**, *110* (2), 733–737.

(96) Jones, M.; Scholes, G. D. On the Use of Time-Resolved Photoluminescence as a Probe of Nanocrystal Photoexcitation Dynamics. *Journal of Materials Chemistry* **2010**, *20* (18), 3533.

(97) Knowles, K. E.; McArthur, E. A.; Weiss, E. A. A Multi-Timescale Map of Radiative and Nonradiative Decay Pathways for Excitons in CdSe Quantum Dots. *ACS Nano* **2011**, *5* (3), 2026–2035.

(98) Huang, S. C.; Stump, M. D.; Weiss, R.; Caldwell, K. D. Binding of Biotinylated DNA to Streptavidin-Coated Polystyrene Latex: Effects of Chain Length and Particle Size. *Analytical biochemistry* **1996**, *237* (1), 115–122.

(99) Huang, S. C.; Swerdlow, H.; Caldwell, K. D. Binding of Biotinylated DNA to Streptavidin-Coated Polystyrene Latex. *Analytical Biochemistry* **1994**, *222* (2), 441–449.

(100) Piletska, E. V.; Piletsky, S. A. Size Matters: Influence of the Size of Nanoparticles on Their Interactions with Ligands Immobilized on the Solid Surface. *Langmuir* **2010**, *26* (6), 3783–3785.

(101) Medintz, I. L.; Mattoussi, H. Quantum Dot-Based Resonance Energy Transfer and Its Growing Application in Biology. *Physical chemistry chemical physics : PCCP* **2009**, *11* (1), 17–45.

(102) Pons, T.; Medintz, I. L.; Sykora, M.; Mattoussi, H. Spectrally Resolved Energy Transfer Using Quantum Dot Donors: Ensemble and Single-Molecule Photoluminescence Studies. *Physical Review B* **2006**, *73* (24), 245302.

(103) Biju, V. Chemical Modifications and Bioconjugate Reactions of Nanomaterials for Sensing, Imaging, Drug Delivery and Therapy. *Chemical Society reviews* **2014**, *43* (3), 744–764.

(104) Allan, G.; Delerue, C. Energy Transfer between Semiconductor Nanocrystals: Validity of Förster's Theory. *Physical Review B* **2007**, *75* (19), 195311.

(105) Zheng, K.; Žídek, K.; Abdellah, M.; Zhu, N.; Chábera, P.; Lenngren, N.; Chi, Q.; Pullerits, T. Directed Energy Transfer in Films of CdSe Quantum Dots: Beyond the Point Dipole Approximation. *Journal of the American Chemical Society* **2014**, *136* (17), 6259–6268.

(106) Biju, V.; Itoh, T.; Baba, Y.; Ishikawa, M. Quenching of Photoluminescence in Conjugates of Quantum Dots and Single-Walled Carbon Nanotube. *The journal of physical chemistry. B* **2006**, *110* (51), 26068–26074.

(107) Bissell, M. J.; Radisky, D. Putting Tumours in Context. *Nature Reviews Cancer* **2001**, *1* (1), 46–54.

(108) Kalluri, R.; Zeisberg, M. Fibroblasts in Cancer. *Nature Reviews Cancer*. 2006, pp 392–401.

(109) Egeblad, M.; Werb, Z. New Functions for the Matrix Metalloproteinases in Cancer Progression. *Nature reviews. Cancer* **2002**, *2* (3), 161–174.

(110) Springman, E. B.; Angleton, E. L.; Birkedal-Hansen, H.; Van Wart, H. E. Multiple Modes of Activation of Latent Human Fibroblast Collagenase: Evidence for the Role of a Cys73 Active-Site Zinc Complex in Latency and A "cysteine Switch" mechanism for Activation. *Proceedings of the National Academy of Sciences of the United States of America* **1990**, *87* (1), 364–368.

(111) Van Wart, H. E.; Birkedal-Hansen, H. The Cysteine Switch: A Principle of Regulation of Metalloproteinase Activity with Potential Applicability to the Entire Matrix Metalloproteinase Gene Family. *Proceedings of the National Academy of Sciences of the United States of America* **1990**, *87* (14), 5578–5582.

(112) Strongin, A. Y.; Collier, I.; Bannikov, G.; Marmer, B. L.; Grant, G. A.; Goldberg, G. I. Mechanism of Cell Surface Activation of 72-kDa Type IV Collagenase. Isolation of the Activated Form of the Membrane Metalloprotease. *The Journal of biological chemistry* **1995**, *270* (10), 5331–5338.

(113) Deryugina, E. I.; Ratnikov, B.; Monosov, E.; Postnova, T. I.; DiScipio, R.; Smith, J. W.; Strongin, A. Y. MT1-MMP Initiates Activation of pro-MMP-2 and Integrin αvβ3 Promotes Maturation of MMP-2 in Breast Carcinoma Cells. *Experimental Cell Research* **2001**, *263* (2), 209–223.

(114) Morrison, C. J.; Butler, G. S.; Bigg, H. F.; Roberts, C. R.; Soloway, P. D.; Overall, C. M. Cellular Activation of MMP-2 (Gelatinase A) by MT2-MMP Occurs via a TIMP-2-Independent Pathway. *The Journal of biological chemistry* **2001**, *276* (50), 47402–47410.

(115) Yao, H.; Zhang, Y.; Xiao, F.; Xia, Z.; Rao, J. Quantum Dot/bioluminescence Resonance Energy Transfer Based Highly Sensitive Detection of Proteases. *Angewandte Chemie - International Edition* **2007**, *46* (23), 4346–4349.

(116) Shi, L.; De Paoli, V.; Rosenzweig, N.; Rosenzweig, Z. Synthesis and Application of Quantum Dots FRET-Based Protease Sensors. *Journal of the American Chemical Society* **2006**, *128* (32), 10378–10379.

(117) Zhao, M.; Josephson, L.; Tang, Y.; Weissleder, R. Magnetic Sensors for Protease Assays. *Angewandte Chemie* **2003**, *115* (12), 1413–1416.

List of Publication for PhD Thesis

1. Fluorescence Quenching of CdSe/ZnS Quantum Dots by using Black Hole Quencher Molecules Intermediated with Peptide for Biosensing Application.

Sreenadh Sasidharan Pillai, Hiroshi Yukawa, Daisuke Onoshima, Vasudevanpillai Biju, Yoshinobu Baba. Cell Medicine, Volume 8, Numbers 1-2, 2015, pp. 57-62(6).

2. Förster Resonance Energy Transfer Mediated Photoluminescence Quenching in Stoichiometrically Assembled CdSe/ZnS Quantum dot –Peptide labeled Black Hole Quencher conjugates for Matrix Metalloproteinase-2 sensing.

Sreenadh Sasidharan Pillai, Hiroshi Yukawa, Daisuke Onoshima, Vasudevanpillai Biju, Yoshinobu Baba, Analytical Science, 2017 vol: 33 (2) pp: 137-142

3. Quantum dot-peptide nanoassembly on mesoporous silica nanoparticle for biosensing.

Sreenadh Sasidharan Pillai, Hiroshi Yukawa, Daisuke Onoshima, Vasudevanpillai Biju, Yoshinobu Baba. (Submitted)

List of Presentation at the Conference

1**.** FRET from Quantum Dot to Black Hole Quencher acceptors in Quantum Dot-Peptide Nanoassembly for biosensing.

Sreenadh Sasidharan Pillai, Hiroshi Yukawa, Daisuke Onoshima, Vasudevanpillai Biju, Yoshinobu Baba, M.A. 2017, 1st International Symposium on Quantum Life Science, 25-26 th July, Tokyo, Japan. Poster

2. Fluorescence turn on Nanobiosensor Quantum Switch for the Sensitive Detection of Matrix Metalloproteinase.

Sreenadh Sasidharan Pillai, Hiroshi Yukawa, Daisuke Onoshima, Vasudevanpillai Biju, Yoshinobu Baba, M.A. 2015. 95th Annual Meeting of the Chemical Society of Japan on 26-29th March 2015, Tokyo, Japan.(Abstract)

3. Fluorescence turn on Nanobiosensor Quantum Switch for the Sensitive Detection of Matrix Metalloproteinase.

Sreenadh Sasidharan Pillai, Hiroshi Yukawa, Noritada Kaji, Vasudevanpillai Biju, Yoshinobu Baba, M.A. 2014. 8th Asian Photochemistry Conference (APC-2014), Trivandrum, India from 10-1 3th November 2014. (Abstract)

4. A Study on the size controlled synthesis and emission spectra of Lanthanide doped upconversion nanoparticle.

Sreenadh Sasidharan Pillai, Yukihiro Okamoto, Hiroshi Yukawa, Noritada Kaji, Yoshinobu Baba, M.A. 2014. 94th Annual Meeting of the Chemical Society of Japan on 26-29 March 2014, Nagoya, Japan.(Abstract).

5. The Development of Lanthanide doped upconversion nanoparticle towards in vivo imaging.

Sreenadh Sasidharan Pillai, Yukihiro Okamoto, Hiroshi Yukawa, Noritada Kaji, Yoshinobu Baba, M.A. 2013, at IGER Annual Meeting 2013 on 8th January 2014, Nagoya University, Japan. Poster